ADVANCED IDENTIFICATION OF FLOW CURVE PARAMATERS IN TENSION TEST

A MASTER'S THESIS

in

Manufacturing Engineering

Atılım University

by

EMRE CORUK

MAY 2011

ADVANCED IDENTIFICATION OF FLOW CURVE PARAMATERS IN TENSION TEST

A THESIS SUBMITTED TO

THE GRADUATE SCHOOL OF NATURAL AND APPLIED SCIENCES

OF

ATILIM UNIVERSITY

BY

EMRE CORUK

IN PARTIAL FULFILLMENT OF THE REQUIREMENTS FOR THE DEGREE OF

MASTER OF SCIENCE

IN

THE DEPARTMENT OF MANUFACTURING ENGINEERING

MAY 2011

Approval of the Graduate School of Natural and Applied Sciences, Atılım University.

_____

Prof. Dr. İbrahim Akman

Director

I certify that this thesis satisfies all the requirements as a thesis for the degree of Master of Science.

_____

Prof. Dr. Bilgin Kaftanoğlu

Head of Department

This is to certify that we have read the thesis "Advanced Identification of Flow Curve Parameters in Tension Test" submitted by "Emre Coruk" and that in our opinion it is fully adequate, in scope and quality, as a thesis for the degree of Master of Science.

_____	_____
Asst. Prof. Dr. Besim Baranoğlu	Asst. Prof. Dr. Celalettin Karadoğan
Co-Supervisor	Supervisor

Examining Committee Members

Prof. Dr. Bilgin Kaftanoğlu	_____
Prof. Dr. Faruk Elaldı	_____
Asst. Prof. Dr. Celalettin Karadoğan	_____
Asst. Prof. Dr. Besim Baranoğlu	_____
Asst. Prof. Dr. Hakan Argeşo	_____

Date:05/05/2011

I declare and guarantee that all data, knowledge and information in this document has been obtained, processed and presented in accordance with academic rules and ethical conduct. Based on these rules and conduct, I have fully cited and referenced all material and results that are not original to this work.

Emre CORUK

ABSTRACT

ADVANCED IDENTIFICATION OF FLOW CURVE PARAMATERS IN TENSION TEST

Coruk, Emre

M.S., Manufacturing Engineering

Supervisor: Asst. Prof. Dr. Celalettin Karadoğan

Co-Supervisor: Asst. Prof. Dr. Besim Baranoğlu

May 2011, (70) pages

Although the tension test is the simplest method to obtain the stress-strain diagrams (and through these diagrams, the flow curves), since it provides less knowledge than required, an extrapolation of data is to be made if the obtained flow curve is intended to be used in modelling a sheet metal forming application.

In a typical tensile test, strains up to unity can be reached, however, due to the instability in the form of necking which hinders mathematical evaluation of stresses and strains from direct elementary measurements, stress-strain relations up to 0.3-0.4 are obtained. To cope with this problem, either approximate/measured neck geometry or the optical measurements of strains at the most stretched material point have been utilized in order to get further information. In these approaches either the strain or the stress distribution is approximated.

In this study, optical strain measurements from all over the most critical section are made. Also, stress values at this critical section are calculated through a preselected material model under the constraint of force balance. This approach eliminates the assumption of uniform stress distribution over the most critical cross-section and provides a more realistic approach. Following the advance of the strain and

corresponding stress values at the most critical section, flow curves that reach the strain values just before the rupture may be attained.

Several flow curves are evaluated using materials which have in-plane isotropy. Obtained flow curves are compared with the results from hydraulic bulge tests, which are also evaluated using optic strain measurements. Results are promising, at least for the ductile materials that are tested within the scope of this study, in the way that expensive and cumbersome hydraulic bulge tests are no more necessary in order to obtain the flow curves up to higher strains.

Keywords: Material characterization, tensile test, optic strain measurement, Hydraulic Bulge Test (HBT).

ÖZ

ÇEKME TESTİ İLE ELDE EDİLEN AKMA EĞRİSİ PARAMETRELERİNİN GELİŞTİRİLMESİ

Coruk, Emre

Yüksek Lisans, İmalat Mühendisliği Bölümü

Tez Yöneticisi: Yrd. Doç. Dr. Celalettin Karadoğan

Ortak Tez Yöneticisi: Yrd. Doç. Dr. Besim Baranoğlu

Mayıs 2011, (70) Sayfa

Sac metallerde gerilme-gerinim diyagramlarını elde etmenin en kolay yolu çekme testidir. Sac metal sekillendirme operasyonlarının çoğunda bu bilgi kullanılmasına rağmen, deneysel olan bu değerleri ekstarpolasyon ile daha yüksek gerinimlere taşımak gerekmektedir.

Çekme testinde gerinim değerleri 1 değerine kadar yükselmesine rağmen ancak çok küçük gerinim değerlerine kadar kullanılabilmektedir. Bunun nedeni çekme testinde oluşan boyun verme ve gerilme-gerinim değerlerini hesaplarken kullanılan matematiksel formüllerin malzemenin boyun vermesinden dolayı geçersiz olmasıdır. Ancak boyun verme geometrisi optik olarak tespit edilebilirse, malzemenin daha yüksek gerinim değerlerine ulaşmasına rağmen hesaplanamayan gerinim değerleri hesaplanabilir. Bu yaklaşım ile çekme testinden daha çok bilgi edenilmesi mümkündür.

Optik gerinim ölçümleri, gerinimin maksimum olduğu bölgede yapılmış olup, gerilim hesapları önceden belirlenmiş anisotropi ve sabit bir sertleşme modeli kullanılarak, ayrıca çekme testi makinesinin ölçtüğü kuvvet değerleri ile eşitliği sağlanarak, akma eğrisi kopmadan hemen önceki gerinim değerlerine kadar bulunmuştur.

Bulunan akma eğrinin doğruluğunu belirleyebilmek için sonlu elemanlar analizi programı kullanarak çekme testi simulasyonları gerçekleştirilmiştir. Bu simulasyonlar yapılırken malzeme girdisi bölümüne elde edilen akma eğirisi girilmiştir. Bu simulasyondan çıkan kuvvet – uzama diyagramı ile çekme testinden elde edilen kuvvet – uzama diyagramı aynı çıkmaktadır. Bu sonuç hesaplama ile bulunanan yüksek gerinimlerdeki akma eğrisinin doğru olduğunu göstermektedir. Daha sonrasında optik gerinim ölçerin verdiği dağılım ile sonlu elemanlar programının verdiği dağılım, eşdeğer plastik gerinimler bakımından karşılaştırılmış ve aynı renk dağılımı ile aynı gerinim değerleri elde edilmiştir.

Son olarak optik gerinim ölçerin verdiği gerinimler ile hesaplanan akma eğrisi, hidrolik şişirme testi sonucunda elde edilen akma eğrisi ile karşılaştırılmıştır. Sonuçda optik gerinim ölçer sayesinde elde edilen akma eğirisi, hidrolik şişirme testinden elde edilen akma eğrisine yakın çıkmıştır. Her iki eğride yüksek gerinim değerlerine kadar ulaşmıştır. Hidrolik şişirme testi yüksek gerinimlerde malzemenin karakteristiğini elde etmek için yapıldığından dolayı pahalı ve yapılması zor olan bu test önemini yitirecektir.

Anahtar Kelimeler: Malzeme karakterizasyonu, çekme testi, optik gerinim ölçümü, hidrolik şişirme testi.

To My Family

ACKNOWLEDGMENTS

Firstly, I would like to express my deepest gratitude and appreciation to my supervisor Asst. Prof. Dr. Celalettin Karadoğan who inspired, encouraged and supported me at all levels of this study. I would not be able complete this thesis without his support and contributions. Then I would like to thank my co-supervisor Asst. Prof. Dr. Besim Baranoğlu for his suggestions and comments.

I send my best wishes to Metal Forming Center of Excellence (MFCE) members for their contributions.

I would like to express my thanks to Prof. Dr. Bilgin Kaftanoğlu head of Atılım University Manufacturing Engineering Department for his help and suggestions.

I also would like to express my thanks to Prof. Dr. A. Erman Tekkaya for advice and suggestions.

I would like to thank to my colleagues Burcu Tolungüç, Sinem Adıgüzel, whose friendship, support and suggestions made great contributions to this work.

Last but not least, I would like to thank my parents, sisters, and my fiance Ece for always being with me before and during this study.

NOMENCLATURE

G	Gage Length
W	Width
T	Thickness
R	Radius of Fillet
L	Over-all Length
A	Length of Reduced Section
B	Length of Gripped Section
C	Width of Gripped Section
σ	Stress
ε	Strain
σ_{eng}	Engineering Stress
ε_{eng}	Engineering Strain
σ_{true}	True Stress
ε_{true}	True Strain
σ_{UTS}	Ultimate Tensile Strength
A_0	Initial Cross Sectional Area
A	Instantaneous Sectional Area
P	Instantaneous Load
ΔL	Increase in Length

L_0	Initial Length of the Specimen
L	Instantaneous Length of the Specimen
τ	Shear Stress
γ	Shear Angle
r	Radial Position
θ	Twist Angle
K	Strength Coefficient
n	Strain Hardening Exponent
ε_0	Strain at Yield Point
σ_0	Yield Stress
ε_{pl}	Plastic Strain
ε_{el}	Elastic Strain
λ	Stretch Ratio
F	Deformation Gradient Tensor
R	Rotation Matrix
U	Right Stretch Tensor
V	Left Stretch Tensor
ε_x	x - Direction Strain
ε_y	y - Direction Strain
ε_{xy}	Shear Strain
ε_1	Major Strain
ε_2	Minor Strain
$\varepsilon_{von-mises}$	Von Mises Strain

ε_{tresca}	Tresca Strain
L	Segment Length
Y_i	Yield Point along *i* Direction
r	Bulge Radius
ρ_H	Hill's Analytical Bulge Radius
ρ_P	Panknin's Analytical Bulge Radius
r_c	Radius of Bulge Piston
h_d	Height of Dome Point
r_f	Fillet Radius of Upper Die of HBT
p	Pressure
t_o	Initial Metal Sheet Thickness
t	Instantaneous Metal Sheet Thickness
n	Material Hardening Exponent
τ_B	Material Shear Strength
F_S	Punch Force
d_c	Punch Diameter

TABLE OF CONTENTS

LIST OF FIGURES

LIST OF TABLES

CHAPTER 1

INTRODUCTION

1.1 Classification of Manufacturing Processes

The manufacturing methods can be classified into five general areas [1]:

- *Primary shaping* processes, such as casting, die casting, melt extrusion and pressing of metal powder. These process, the materials initially have no shape but obtains a well-defined geometry.
- *Forming* processes, such as rolling, extrusion, cold and hot forging, deep drawing and bending, where material is formed under the application of forces. In these applications the material cohesion is not broken (no melting or cutting is in place).
- *Material removal* processes, such as turning, milling, broaching and sawing where removing material generates a new shape.
- *Property enhancement / Surface treatment* processes, such as heat-treating, anodizing and surface hardening, where the part remains essentially unchanged in shape but undergoes change in properties or appearance.
- *Joining processes,* Permanent Joining Processes, such as welding, brazing, soldering and adhesion. These processes joint result in permanent (irreversible) joining of components. Mechanical joining processes, such as riveting, shrink fitting and mechanical assembly. These processes bring two or more parts together to build a subassembly which can, when intended, be disassembled without any damage to the components.

1.2 Metal Forming Processes

The term metal forming refers to a group of manufacturing methods by which the given material is transformed into a useful part without change in the mass or composition of the material.

Among all manufacturing processes, metal forming technology has a special place because it allows the production of parts of the best mechanical properties with minimum waste of material. In most metal forming processes initial material shape is simple. The material is plastically deformed in one or more operations into a product of relatively complex shapes. Forming to near net or net shape dimensions reduces metal removal requirements, resulting in significant material and energy savings [1].

The metal forming can be classified into two general areas:

- Massive (bulk) forming processes such as forging, extrusion, rolling and drawing etc...
- Sheet forming processes such as deep drawing, stretch forming etc…

1.3 Definition and Necessity of Flow Curve in Metal Forming Processes

The modeling of metal forming processes requires a suitable plastic deformation model and the information on the dependence of the equivalent stress with respect to the equivalent strain within the plastic deformation zone. The equivalent stress - equivalent strain relationship (from this point on, the term stress-strain relation will be used) can be determined through carefully conducted experiments under controlled conditions. Since this relationship is sensitive to mainly temperature and strain-rate, tests needs to be carried out over a range of these parameters in accordance with the actual parameters expected within the forming process being investigated. Such material properties at room and elevated temperatures are needed for processes such as rolling, extrusion, forging and other bulk and sheet forming applications.

There are two main reasons for the accurate determination of the stress-strain curves: Firstly, in order to calculate the forces required for metal forming processes it is necessary to know the stress-strain curve of the metals to be formed. Secondly, flow curves will be used in FEM simulations.

The final dimensions and stress-strain distribution of the workpieces have to be obtained from the modeling of experiments very close to reality. Therefore it is very important to obtain flow curves correctly. Tension and compression tests are the most popular material flow characterization tests in metal forming. Tension test is the best-described test, but supplies a flow curve up to lower strain values than the compression test does. The tension and compression tests are explained in following sections in detail.

1.4 Aim and Scope of the Thesis

Tension test is the simplest way to obtain stress-strain diagrams for sheet metals. Analysis of almost all practical sheet metal forming applications, however requires an extrapolation of the experimental stress-strain values. As it is well known, the reason is the instability in the form of early necking, encountered during the tension test. This phenomenon hinders the post-diffuse-necking computation of stresses and strains based on the elementary measurements of force and extension in the axial direction. As an alternative hydraulic bulge test can be used. Due to its biaxial nature, diffuse necking in the hydraulic bulge test is skipped and the instability appears first in the form of local necking. For this reason, and also due to its biaxial nature hydraulic bulge test provides experimental data up to higher strains when compared to that from tension test. A closer investigation however shows the fact that; comparable strains are attained also during the tension test. Approximated or measured neck geometry, optical measurements of strains at the most stretched material point have been utilized in order to get some more information from the tensile test. In all these approaches either the strain or the stress distribution is approximated or assumed to be uniform along the *most critical section* (cross section in which the most strained material point situated).

Aim of this thesis is optical strain measurements around the most critical section, and stress computations based on a yield criteria under constraint of force balance reveals the flow curve up to attained strain values just before the rupture occurs. This approach is one step further, which also eliminates the assumption of uniform stress distribution over the most critical cross section.

Several flow curves are evaluated using materials which have in-plane isotropy. Obtained flow curves are compared with the results from tension tests done by precise tangible extensometers and also by hydraulic bulge tests, which are evaluated using optical strain measurements as well. Furthermore, extension-force diagrams obtained from simulation of the tension tests using the obtained flow curves are in good agreement with the experimental values. Therefore, the approach is promising, in the way that expensive and cumbersome hydraulic bulge tests are not any more necessary in order to obtain the flow curves up to higher strains.

CHAPTER 2

LITERATURE SURVEY

2.1 Introduction

In this chapter the previous literature related to the current study will be discussed. First, the flow curve determination methods will be introduced. Then the approximations of flow curve, digital image correlation for optical strain measurement and finite element method, determination of the flow curves, will be explained.

2.2 Flow Curve Determination Methods

In the forth-coming sections, various methods for flow curve determination will be introduced. Advantages and disadvantages of these methods will be explained.

2.2.1 Tensile Test (or Uniaxial Tension Test)

The Tensile Test consists of pulling a sample of material (with a pre-defined standard geometry) under a load until it breaks down into two parts (fracture). The static uniaxial test is probably the simplest and the most widely used mechanical test. The results of tensile tests are used in many areas in engineering applications. The Tensile Test is performed at room temperature or at an elevated temperature with some specific tools and machines. Outputs of the Tensile Test are elongation, yield strength, yield strength elongation, tensile strength and reduction area, etc.

Advantages and Disadvantages of the Tension Test

- Tension tests provide information on the strength and ductility of materials under uniaxial tensile stresses. This information may be useful in comparisons of materials, alloy development, quality control, and design under certain circumstances.
- These test methods are considered satisfactory for acceptance testing of commercial shipments. The test methods have been used extensively in the trade for this purpose [3].
- Determination of outputs can be presented in many ways however; plotting engineering stress-strain diagram is the most common way. A sample engineering stress-strain curve is established from load-elongation measurements.
- Necking limits uniform the elongation in tension, making it difficult to study plastic stress–strain relationships at high strains [2].

Test Specimen

Test specimen can be substantially full size machined. Improperly prepared test specimens are often the reason for incorrect results. The important part of the specimen is the gauge section. The cross-sectional area of the gauge section is less than that of the shoulders and grip region, so the deformation will occur here. The gauge section should be long compared to the width (typically four times). The transition between the gauge section and the shoulders should be at least as great as the diameter so that the larger ends do not constrain the deformation in the gauge section. Description for test specimen dimensioning is given in ASTM Standards E8-04 (see Figure 2.1).

G: Gage Length
W: Width
T: Thickness
R: Radius of Fillet
L: Over-all Length
A: Length of Reduced Section
B: Length of Gripped Section
C: Width of Grip Section

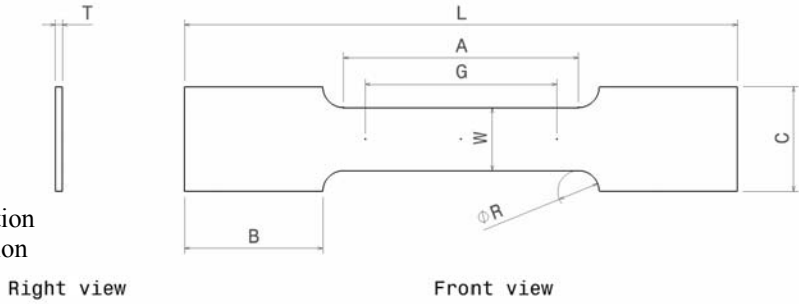

Figure 2.1 Tensile test specimen

A typical metallic specimen undergoes different deformation stages during tensile test. Firstly, the elastic deformation where no permanent shape change is observed. Then at a point that is beyond the yield point, metal starts to deform plastically where the deformation now is permanent. During this permanent deformation, material elongates uniformly and this deformation is called "uniform elongation". During this uniform elongation, the metal is work hardened and higher forces are required to further deform the metal [5].

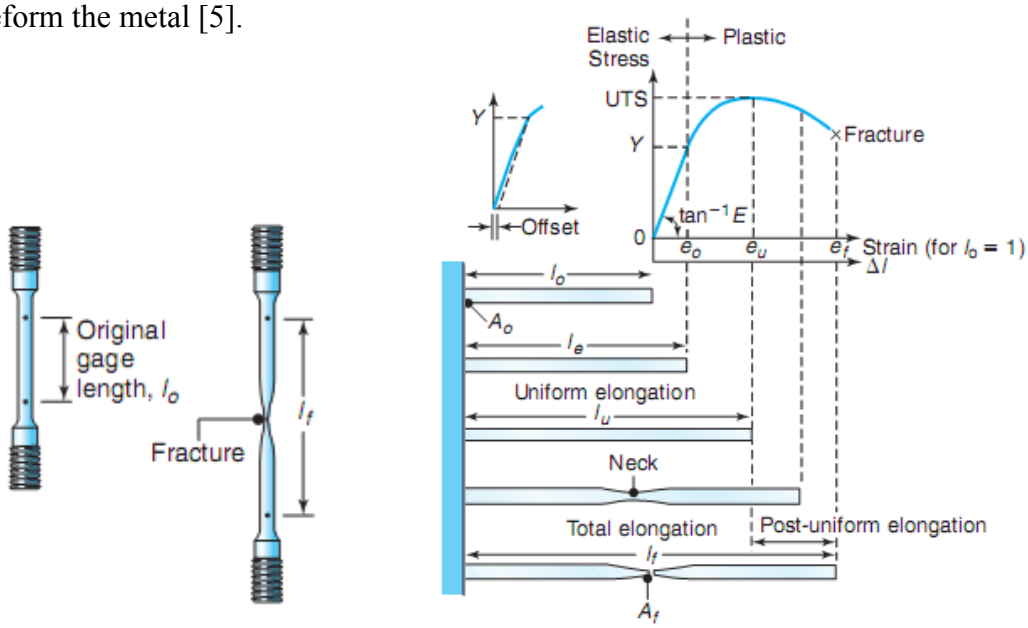

Figure 2.2 Deformation steps [4]

- Engineering Stress-Strain Curve

The engineering stress (nominal stress) is defined as the ratio of the applied load, P, to the original cross-sectional area, A_0, of the specimen:

$$\sigma_{eng} = \frac{P}{A_0} \tag{2.1}$$

The engineering strain is defined as

$$\varepsilon_{eng} = \frac{\Delta L}{L_0} = \frac{L_f - L_0}{L_0} \tag{2.2}$$

where is L_f the instantaneous length of the specimen, L_0 the initial length of the specimen.

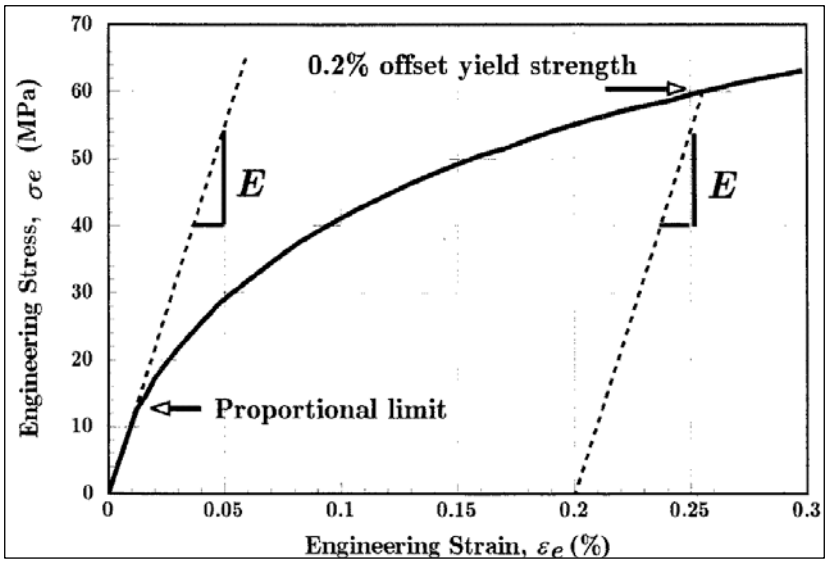

Figure 2.3 Engineering Stress vs. Strain Diagram [3]

The parameters that are used to describe the stress-strain curve of a metal are the ultimate tensile strength, yield point, percent elongation and reduction in area.

- Ultimate Tensile Strength

The ultimate tensile strength is the maximum load of a stress-strain curve divided by the cross sectional area of a specimen. A marked decrease in cross-section is called "necking." Ultimate tensile strength (UTS) is another commonly used term for tensile strength [2-5].

$$\sigma_{UTS} = \frac{P_{\max}}{A_0} \tag{2.3}$$

- Yield Point

Yield point meaning of identifying the stress at which plastic deformation begins. The stress at which plastic deformation or yielding is observed to begin depends on the sensitivity of the strain measurements. Thus in the elastic range, strain is measured using an “extensometer”.

- Offset Yield Point

This is the most widely used strength measure of metals. A plastic strain of 0.2% is usually used to define the offset yield stress, although other values may be used depending on the material and the application. In some materials there is essentially no linear region and so a certain value of strain is defined instead. Although somewhat arbitrary, this method does allow for a consistent comparison of materials [6].

- Percent Elongation

Elongation shows the total increase in specimen’s length from yield point to fracture (rupture). Total elongation is determined by broken and original specimen measurements. In general, metals elongate 30-50% [5]. Elongation does not show formability because for the same material with different specimens, elongation may change.

- Modulus of Elasticity

Metal deformation is proportional to the imposed loads over a range of loads. Since stress is proportional to load and strain is proportional to deformation, this implies that stress is proportional to strain. Hooke's Law is the statement of that proportionality.

$$\sigma = E\varepsilon \tag{2.4}$$

- True Stress-Strain Curve

Engineering stress is based on the original cross-sectional area, A_0, of the specimen. However, the instantaneous cross-sectional area of the specimen becomes smaller as it elongates, just as the area of a rubber band does; thus, engineering stress does not represent the actual stress to which the specimen is subjected [4].

True stress is defined as the ratio of the load, P, to the actual (instantaneous, hence true) cross-sectional area, A, of the specimen:

$$\sigma_{true} = \frac{P}{A} \tag{2.5}$$

Strain measurement is often used in conjunction with true stress data that takes the incremental increase in displacement not the original one.

$$d\varepsilon_{true} = \frac{dL}{L} \Rightarrow \varepsilon_{true} = \int_{L_0}^{L} \frac{dL}{L} = \ln \frac{L}{L_0} \tag{2.6}$$

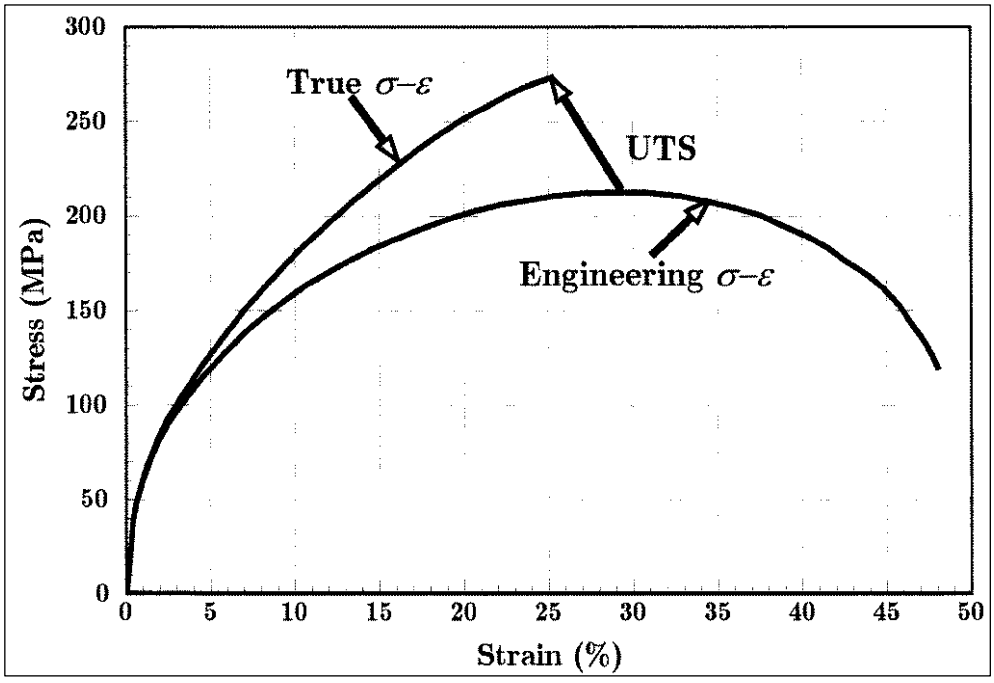

Figure 2.4 Comparison of True and Engineering Stress-strain curves [3]

Hence, true and engineering stress are related by,

$$\sigma_{true} = \sigma_{eng}\left(\frac{A_0}{A}\right) \tag{2.7}$$

Hence, true and engineering strains are related by,

$$\varepsilon_{true} = \ln\left(\frac{L_0 + \Delta L}{L_o}\right) = \ln\left(1 + \frac{\Delta L}{L_0}\right) = \ln(1 + \varepsilon_{eng}) \tag{2.8}$$

The volume in a tension test change but this is very limited. It is therefore reasonable to take the volume as constant.

$$A_0 L_0 = AL \tag{2.9}$$

This gives,

$$\frac{A_0}{A} = \frac{L}{L_0} = \frac{L_0 + \Delta L}{L_0} = 1 + \varepsilon_{eng} \tag{2.10}$$

Substitution of the above equation in Eq. (2.8) gives:

$$\varepsilon_{true} = \ln\left(\frac{A_0}{A}\right) = \ln(1 + \varepsilon_{eng}) \tag{2.11}$$

- Strain at Necking in a Tension Test

If the behavior of the material in a tension test is ductile, a phenomenon called necking usually occurs. The deformation is uniform along the gage length early in

the test, but later begins to concentrate in one region, resulting in the diameter there decreasing more than elsewhere. In ductile metals, necking begins at the ultimate strength point, and the decrease in load beyond this point is a consequence of the rapidly decreasing cross-sectional area [7].

Assuming that the material behaves according to the well-known Ludwig approximation the true strain at the onset of necking is numerically equal to the strain-hardening exponent, n, of the material [5]. Thus, the higher the value of n, the higher the strain that a piece of material can experience before it begins to neck.

2.2.2 Compression Test

Many operations in manufacturing are performed with the workpiece subjected to compressive stress. The compression test, in which the specimen is subjected to a compressive load, gives useful information on the forces and power requirements in metal forming processes. This test usually has done compressing cylindrical specimen between two well – lubricated flat set of compression dies.

Advantages and Disadvantages of the Compression Test

- Necking problem does not occur in this test. Therefore, much higher strains can be reached in compression tests.
- Friction effect is the very important source of lubricant error in this test. If a good lubricant is used, the error can be minimized. Some preferred lubricants are Teflon® or machine oil at room temperature and at hot working temperatures, graphite in oil for aluminium alloys, and glass for steel, titanium, and high – temperature alloys [1]. Another method to minimize the friction effects is using, different compression test approaches. Some most common methods are Cook & Larke and Rastagaev compression tests.
- Another disadvantage is the barrelling effect on the specimen. Increasing h/d reduces the effect of friction, but this time the specimen will buckle if it is too long and slender. Buckling is likely if the height-to-diameter ratio is greater than

about 3. If the specimen is so well lubricated that the ends of the specimen can slide relative to the platens, buckling can occur for h/d ≥ 1.5 (Figure 2.5) [2].

- Other errors in the compression test can be classified in three categories.
    - Errors in the displacement readings, which results in errors in the calculated strain
    - Errors in the load readings, which results in errors in the calculated stress
    - Errors in the processing of the data due to barrelling of the test specimens

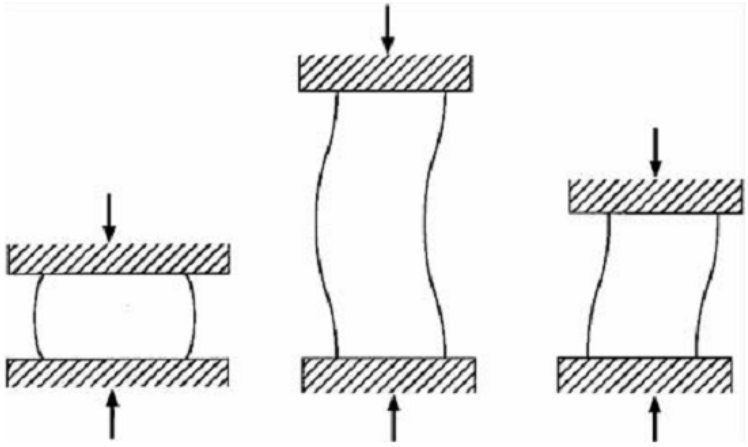

Figure 2.5 Problems with Compression Testing [2]

Stress and Strain Calculations in Compression Test

Similar to the uniform elongation zone of the tensile test, the following relationships are valid for the uniform compression test:

$$\varepsilon_{true} = \ln(\frac{h_o}{h}) = \ln(\frac{A}{A_0}) \tag{2.12}$$

$$\sigma_{true} = \frac{P}{A} \tag{2.13}$$

$$A = A_o(\varepsilon_{eng})^{\varepsilon_{true}} \tag{2.14}$$

Where h_0 and h are initial and instantaneous heights and A_0 and A are initial and instantaneous specimen surfaces areas, respectively.

2.2.3 Hydraulic Bulge Test

Higher strains are attained by using hydraulic bulge test than in uniaxial tension test. A sheet specimen is placed over a circular hole, clamped, and bulge outward by oil pressure acting on one side (Figure 2.6).

Bulge test enables to obtain larger strain values than two times of that is obtained in standard tensile test. So, hydraulic bulge test is used to obtain formability, in sheet quality and also to determine ductility and flow stress curve of the sheet material under biaxial deformation state.

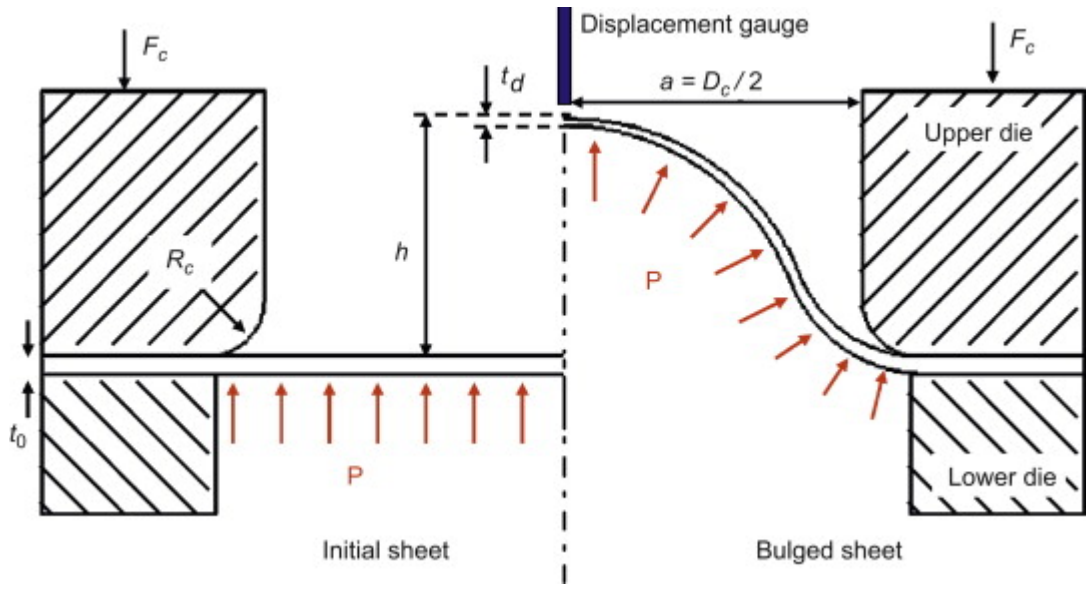

Figure 2.6 Schematic diagram of the bulge setup [8]

In order to investigate the plasticity and strength of sheet metals quasi-static bulge test was developed in the late of 1940s. Chakrabarty and Alexander [9] used Tresca's yield criterion and flow rule to study bulging of circular diaphragms by the help of pressurized fluid and they obtained well theoretical results which match with the

experimental results. Atkinson [10] developed formulations related with thickness variation and radius of curvature near the pole of the radius. Gutscher et al [11] introduced viscous pressure bulge test (VPBT) to obtain flow stress under biaxial stretching conditions. They also carried out FEM simulations and experimental procedures to determine some variables such that dome wall thinning, dome radius, dome height, strain hardening coefficient and anisotropy. Broomhead and Grieve [12] performed studies related with the effects of strain rate for the fracture of sheet metals using bulge test. Pikett et al [13] performed similar studies for high strength steels (HSS). Grolleau et al [14] developed a dynamic bulge test on sheet metals at high strain rates with viscoelastic nylon bars on aluminium sheets for plastic rates up to $500s^{-1}$.

2.3 Approximation Functions of Flow Curves

The flow curve of many metals in the region of uniform plastic deformation can be expressed by the power law equation:

$$\sigma = K\varepsilon^n \tag{2.17}$$

where n is the strain hardening exponent, and K is the strength coefficient. The strain hardening exponent may have values from n=0 (perfectly plastic solid) to n=1 (elastic solid). For most metals, n has values between 0.1 and 0.5 [5].

Another well-known empirical relation is Swift's equation:

$$\sigma = K(\varepsilon_0 + \varepsilon)^n \tag{2.18}$$

ε_0 can be considered to be the amount of strain that the material received prior to the tensile test (initial strain).

Another common validation on is the Ludwick equation:

$$\sigma = A + B(\varepsilon)^m \tag{2.19}$$

where m is the work-softening exponent, and A, B are the material constants. The term A is often called as the initial stress.

Finally, Voce proposed an exponential equation in the form:

$$\sigma = A - (A - B)\exp(-C\varepsilon) \tag{2.20}$$

Where A, B, C are the material constants. This equation mainly is used for the flow curve calculation of aluminum alloys.

2.4 Basics of Digital Image Correlation (DIC)

Optical measurement devices have been increasingly applied in recent years for various materials to characterize their mechanical behavior. Optical measurement systems measure the displacement or strain without contact, using digital image correlation between several sequentially taken images (photos). DIC is an optical metrology method based on digital image processing and numerical computing.

Digital image correlation can be 2D and 3D. The three dimensional digital image correlation technique presented is based on two dimensional technique developed by Sutton et al. (1986) [15].

Table 2.1 Overview of 2D and 3D-DIC properties [16]

	2D	3D
Number of Cameras	1	2
Calibration requirement	No, however needed and possible to gain information on displacement	Yes
Influence of out-of-plane movements of the specimen	Significant influence on strain measurement	No influence on strain measurement
Out-of-plane measurement	Down to 1mm2	Limited by the size and position camera to each other

As shown in Fig 2.8 the principle of any DIC system is to use the random gray value intensity distribution of the pattern on the object and to overlay a grid of subsets or facets on it. The pattern is produced by a black graphite spray so that the specimens are homogeneously covered with densely yet distinctly spaced graphite [16].

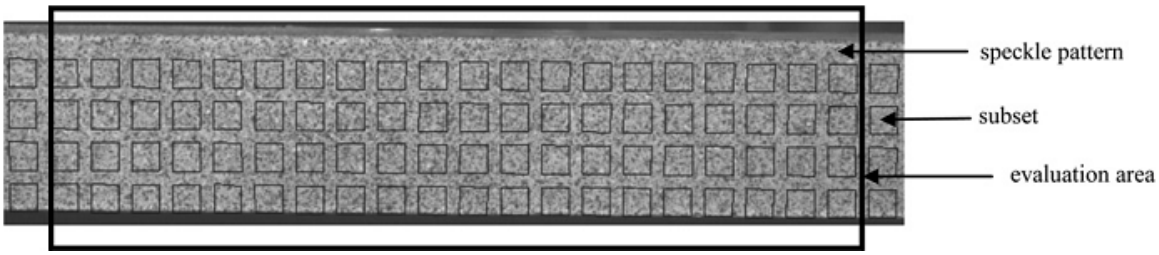

Figure 2.7 The random speckle pattern and the predefined subsets positioned by the software [16]

In the two pictures recorded simultaneously by the cameras, each subset has a unique intensity distribution. The calibration function enables the detection of the position of each subset in three dimensional space. In a series of images recorded during a test, the pattern becomes deformed in accordance with the specimen deformation, and the subsets can be detected in each image according to the intensity distribution calculated and determined in the reference image. As the size and shape of the subsets changes when the target object is strained, the strain field on the specimen surface in longitudinal and transverse direction may be obtained by continuously analyzing the speckle pattern and the deformed subsets. The algorithm applied to identify the subsets in each picture is of great importance for the accuracy of the strain field [16-17-18].

From the numerous software specific adjustable parameters of a DIC system, the most important one affecting the result accuracy is the size of the subsets [19]. As the subset size determines and is equivalent to the minimum local gage length, and since there is no systematic procedure, the definition of an adequate subset size is based on operator experience and judgment. Longitudinal and transverse strain values are obtained for each of the subsets, implying constant strain values within a given subset.

2.5 Previous Works on Tensile Test by Using Optical Measurement Systems

In this section, surveys of previous works which are based on tensile test by using optical measurement systems will be presented. Along with the researches on these areas, studies on solution methods are also investigated.

Tensile testing machine was built in 1824 by Gabriel Lame. First optical device was used for the gage measurement in 1915 by E. M. Eden. Peters W.H. and Ranson W. F. were done digital imaging techniques in experimental stress analysis in 1982 [5] .

M. Jerabek et al. [16] studied, the limits of accuracy of this optical strain measurement system under different environmental conditions, and the technique was applied to the mechanical characterization of polypropylene (PP) and PP composites (PP-C) in the pre- and post-yield regimes. Regarding accuracy, a fine speckle pattern and a light intensity just below overexposure provided best results. In characterizing the transverse strain behavior of PP-C, DIC results exhibited smaller values compared to transverse strains determined utilizing a mechanical clip-on extensometer. The latter effect is attributed to viscoelastic creep indentation of the extensometer pins, which mechanically interact with the specimen via the clip-on spring forces of the extensometer, into the surface. For the DIC system, it could be shown that it is applicable for the proper strain determination both in the pre- and post-yield regimes, and in terms of longitudinal and transverse strains as well as in terms of global average and local strains.

F. Grytten et al. [20] studied, the experimental investigation of the mechanical behavior of a talc and elastomer modified polypropylene compound subjected to large strains. 3D digital image correlation with two cameras and stereo-vision was used to determine full-field displacements during uniaxial tensile tests on specimens with rectangular cross-section.

Jinlong Chen et al. [21] studied, the two-step extended digital image correlation (X-DIC) is proposed to directly measure full-field displacement with discontinuities by using the partition of unity method as the extended finite element method (X-FEM). The displacement variable in the correlation factor of the DIC method was expressed

by the extended finite element displacement mode; in this way, the two-step X-DIC method combined the basic principle of X-FEM with the DIC method.

A new method is used to determine the true stress–true strain curve by Damoulin S. et al [22]. As this method still makes use of a tensile test, the results are compared with the results obtained with an extensometer on a copper sample for which the strain between the grips is supposed to be homogeneous. The calculated strain field brings into evidence an increasing heterogeneity at high deformations. Taking this heterogeneity into account allows a more precise computation of the equivalent stress–equivalent strain curve which is used in a finite element simulation of the tensile test. Comparing the results of the simulation with those of image analysis, it appears that a corrected equivalent stress-equivalent strain relationship is sufficient to obtain a correct behavior up to necking. The simulation also shows that the necking in the material is obtained when a necking criterion (Conside `re's criterion) is verified.

Tensile fracture properties of polycarbonate (PC) and the alloy of poly-carbonate and acrylonitrile–butadiene–styrene (PC/ABS) are experimentally investigated by Qin Zhi Fang et. al. [23]. Two digital cameras are used to record simultaneously the tensile deformation of specimens and the large deformation and the necking process of these polymers are discussed. Two lateral contractions are not identical at the later tensile stages and the contraction ratios in each lateral direction are related with the tensile strains in axial direction on width and thickness surface. The curvature radiuses at the minimum section during necking process are shown. The volume increases during necking process and then decreases gradually.

The efficiency of the digital image correlation method for measuring in-plane displacements in the presence of high strain gradient is presented by Fabienne Lagattu et al. [24]. Three types of strain gradient have been studied: strain localization around a hole in a composite laminate, strain concentration at a crack tip in a TiAl alloy, and strain gradient on a polymer neck front. These three applications concern various materials, various types of loading, and various gradient values.

Y. H. Zhao et al. [25] used experimental results and finite element modeling (FEM) to critically evaluate the influence of the specimen dimensions and strain measurement methods on the tensile curves obtained from miniature specimens. Using coarse-grained Cu as a model material, the results demonstrate that the values of strain obtained from the crosshead displacement are critically influenced by the specimen dimensions such that the uniform elongation and the post-necking elongation both increase with decreasing gauge length and increasing specimen thickness.

Julien Réthoré et al. [26] used, an image correlation algorithm accounting for discontinuities. It is based on a decomposition of the displacement field onto a regular finite element basis supported by a uniform mesh, enriched with suitable functions to describe accurately discontinuities, paralleling recent developments of extended finite elements. This algorithm is applied to a bolted assembly where interface slip is observed upon loading.

V. Tarigopula et al. [27] used a different method. Digital image correlation was used together with high-speed photography to study strain localization in the tensile specimens at high rates of strain. By using digital image correlation, it is possible to obtain in-plane displacement and strain fields during non-uniform deformation of the gauge section, and accordingly the strains associated with diffuse and localized necking may be determined. The full-field measurements in high strain-rate tests reveal that strain localization started even before the maximum load was attained in the specimen. An elasto-viscoplastic constitutive model is used to predict the observed stress–strain behavior and strain localization for the dual-phase steel. Numerical simulations of dynamic tensile tests were performed using the non-linear explicit FE code LS-DYNA. Simulations were done with shell (plane stress) and brick elements. Good correlation between experiments and numerical predictions was achieved, in terms of engineering stress–strain behavior, deformed geometry and strain fields.

F.M. Sánchez-Arévalo and G. Pulos [28] studied the mechanical behavior of three materials: commercial aluminum, bovine pericardium and Cu–Al 11.2 wt.%–Be 0.6

wt.% shape memory alloy. These materials were subjected to simple tension test using an MTS load frame with an attached optical microscope. Displacement, force, strain data and digital images of the sample's surface were acquired. Data and images were post-processed in order to measure displacement vector fields for each material. Local and global strain measurements were done, hence the Young's Modulus was obtained for each material.

Sören Ehlers and Petri Varsta [29] presents a procedure to determine an element-length dependent strain and stress relation until fracture that is suitable for implementation in finite element models. This material relation is obtained experimentally with an optical measuring system. The strain until fracture is calculated from the measured surface displacements. The stress is derived from the measured force and the cross-sectional area in the necking region. Furthermore, because of the digital nature of the optical measurements, the strain reference length, being a function of the pixel size, is clearly defined. For the numerical simulation the finite element length is equal to this strain reference length. The overall procedure allows a precise numerical simulation of the tensile experiment until the point of fracture without curve fitting or an iterative procedure to adjust the material relation for the chosen mesh size. This precise material relation can improve non-linear numerical simulations.

CHAPTER 3

OBTAINING FLOW CURVE STEEL ST12 FROM TENSION TEST USING DIC & FEM

3.1 Introduction

In this chapter, large strain flow curve of material St12 will be determined. This bearing steel is supplied from ORS Bearing Company (Ankara, Turkey) in cold rolled condition. First, the material flow curve is obtained by using tensile test machine and optical strain measurement system. Then the experimental strain data is given computer code so the large strain flow curve is found. Finally, the results are compared with the hydraulic bulge test results. The modelling of these experiments is explained and the conclusions on the success of large strain flow curve are presented.

3.2 Test Method

Material and Sample Preparation

The material investigated in this chapter is commercial steel used for bearing parts. The composition of the St12 (EN 10130) steel employed in this research is 0.003C, 0.161Mn, 0.005P, 0.007S, 0.005Si, 0.037Al, 0.057Ti, all numbers are given in mass fraction (%).

Tensile test specimens are prepared by using ASTM E-8 (Room Temperature Tensile Test) standards. The thickness of the specimens is 1.5 mm.

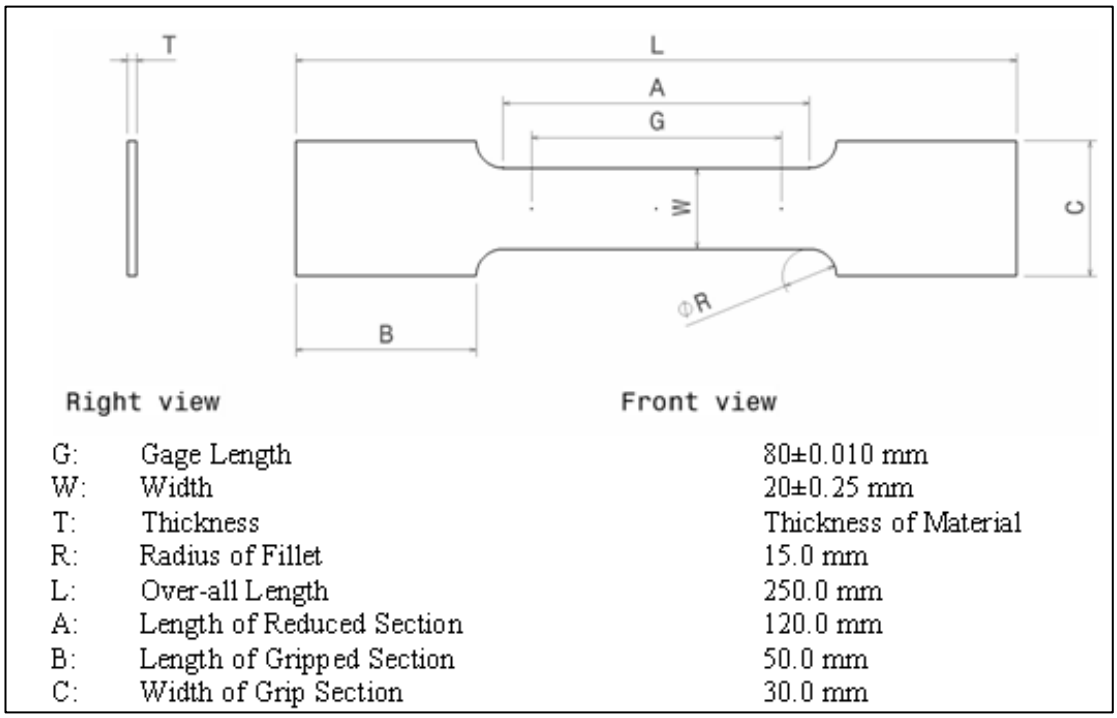

G:	Gage Length	80±0.010 mm
W:	Width	20±0.25 mm
T:	Thickness	Thickness of Material
R:	Radius of Fillet	15.0 mm
L:	Over-all Length	250.0 mm
A:	Length of Reduced Section	120.0 mm
B:	Length of Gripped Section	50.0 mm
C:	Width of Grip Section	30.0 mm

Figure 3.1 Tensile test specimen (ASTM E-8) [30]

A random black and white speckle pattern is applied to front side of the specimen prior to testing using mat spray paint (Figure 3.2).

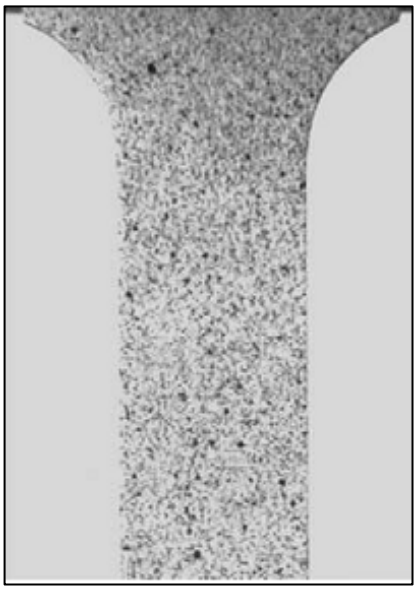

Figure 3.2-Painted Sample

Experimental Procedure

Tensile tests are carried out in a Zwick//Roell Z300E universal test machine at room temperature using constant cross head speeds of 50 mm/min. The gage length of the specimen is 80 mm, resulting in nominal strain rates of 0.01 s^{-1}. The load is measured with a 300 kN load cell [31].

Commercial Aramis digital image correlation (DIC) systems from GOM which are used to measure the displacement field during loading. Two high-resolution cameras (2358 * 1728 pixels) with Titanar 65mmf/2.8 lenses are used [32]. The cameras are mounted on a tripod and arranged so that adjacent face of the specimens is visible to both cameras simultaneously (Figure 3.3a). Unlike 2D DIC systems which do not require any calibration for strain calculations, 3D DIC systems require a system calibration for both strain and displacement calculations [33]. A complete system calibration is run before each experiment to ensure accurate results. A plate with a pre-defined pattern of circular dots is moved around in the measurement area while both cameras acquired several synchronized calibration images (Figure 3.3b).

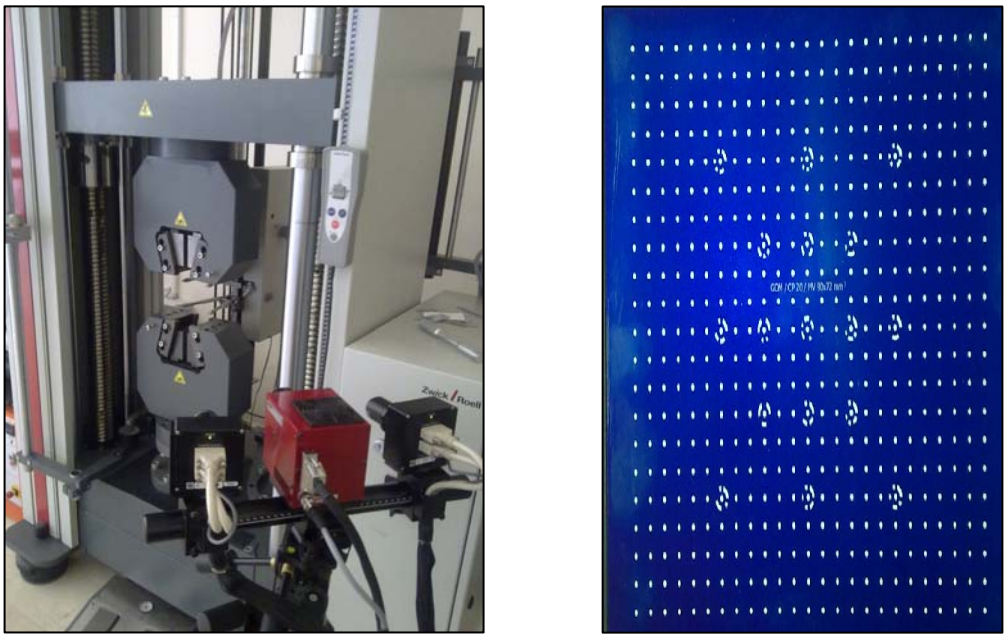

(a) **(b)**

Figure 3.3 (a) Gom-Aramis system is placed in front of the tensile testing machine which is the same time equipped with tangible extensometers. (b) Gom-Aramis calibration plate

Since the spacing between the dots on the calibration target is known, all key parameters of the pin-hole projection based stereo vision model could be determined (Figure 3.4).

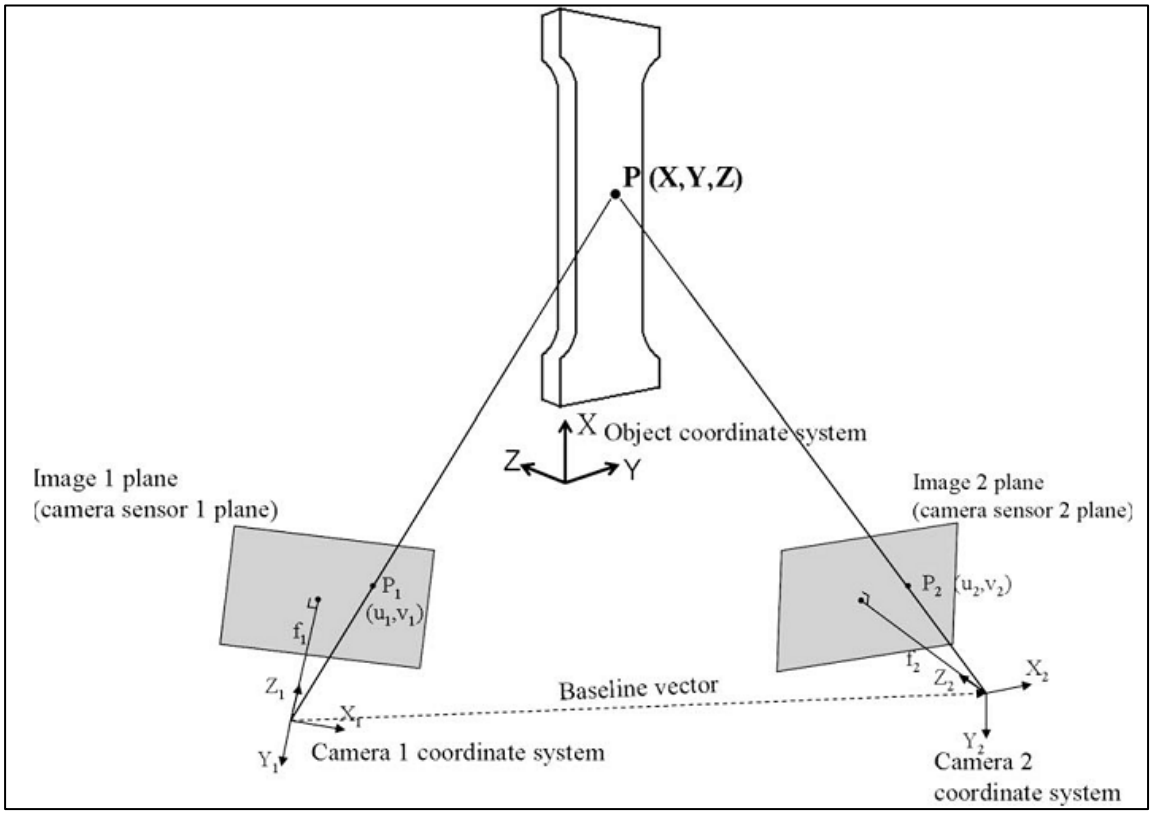

Figure 3.4 Schematic of a two-camera stereo-vision system based on the pinhole projection model [20]

These parameters include the distance from the projection centre to the sensor plane for both cameras, the coordinates of the point where the optical axis intersects the sensor for both cameras, the scale factors relating pixel coordinates to metric distances in both principal direction of the sensor coordinate system and, finally, the relative placement and orientation of the two cameras. A more detailed description of the calibration procedure can be found in e.g. Tiwari et al. [34].

3.3 Measurements

Tensile Testing Machine (Zwick Z300E) Measurements

Tensile test are repeated three times to ensure repeatability. The results are very close to each other so, one of them is chosen in the test results. This result is used all progress. The other results are given in the APPENDIX A. Experimental output has been taken as a force displacement curve, saved by the testing machine on a notepad in ASCII format. Force and displacement curve is drawn by using the program Microsoft Excel (Figure 3.5).

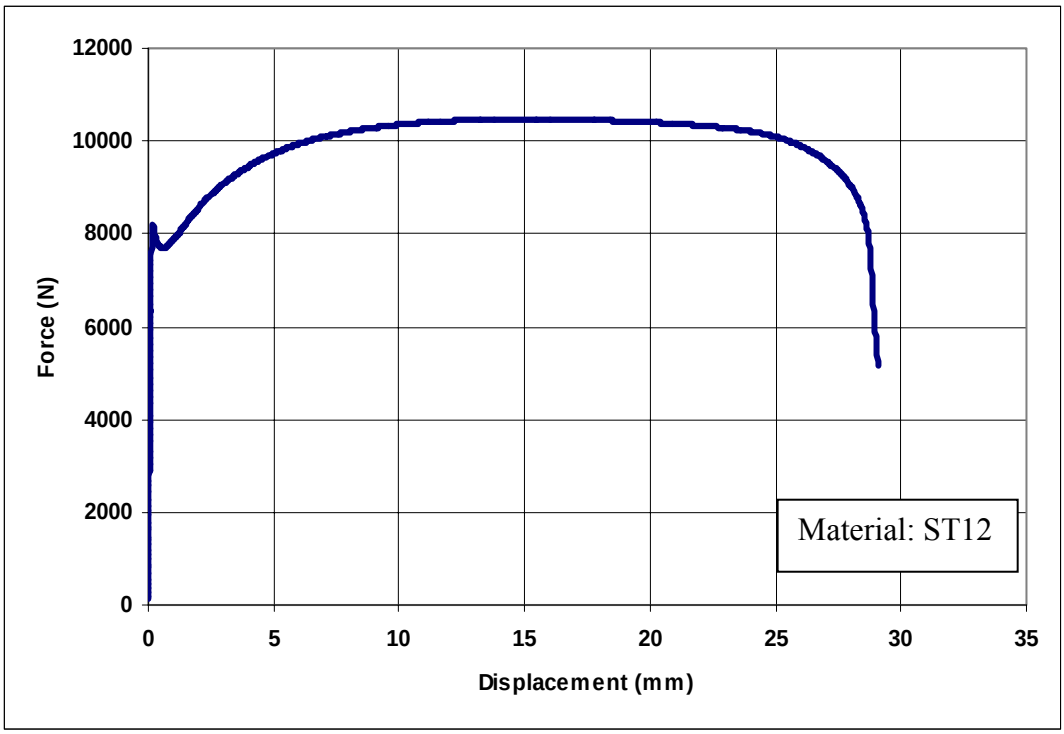

Figure 3.5 Tension test force displacement curve

Force-displacement data can easily be converted to engineering stress – engineering strain data with the help of Eqs. (2.1), (2.2) and to true stress- true strain data with the help of Eqs. (2.5), (2.7). Point of maximum stress on engineering stress-strain curve gives the point where the necking starts and the ultimate tensile strength, σ_{UTS} as shown in Figure 3.6.

For the St12 specimen, ultimate tensile strength can be taken as σ_{UTS} =348 MPa, and necking strain as $\varepsilon_{eng}^{necking}$ =0.18

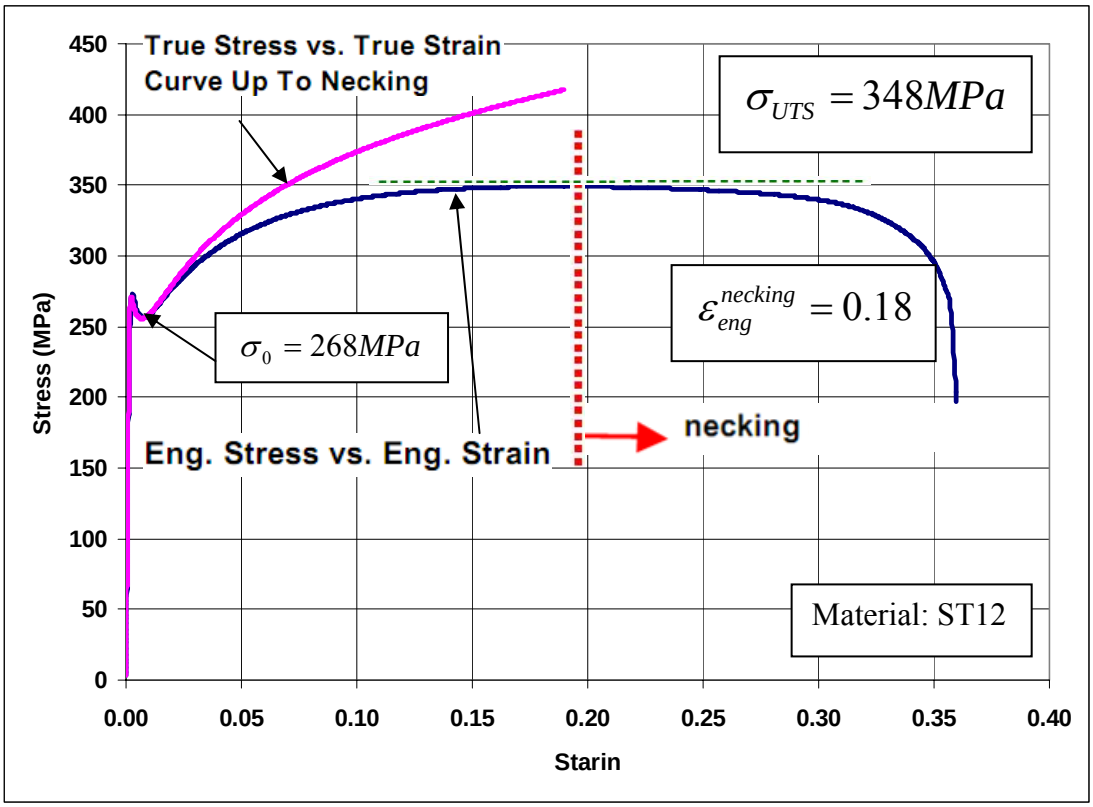

Figure 3.6 Stress and strain curve of material ST12 obtained from tensile test

Material response is clear at the yield point region; therefore, 0.2 % offset strain method is not used to define the yield stress for this material. It is shown to be $\sigma_0 = 268MPa$ on Figure 3.6.

The flow curve can be obtained by plotting true stress values against corresponding equivalent true plastic strain values determined by the Eq. (3.1).

$$\varepsilon_{pl} = \varepsilon_{true} - \varepsilon_{el} = \varepsilon_{true} - \varepsilon_0 - (\frac{\sigma_{true-}\sigma_0}{E}) \qquad (3.1)$$

In this equation, ε_{pl} denotes the total equivalent plastic strain ε_{el} is the total elastic strain, σ_0 is the initial yield stress, ε_0 is the true strain at initial yield point and E is

the modulus of elasticity. Figure 3.7 shows the flow curve of St12 obtained from tension test without any extrapolation.

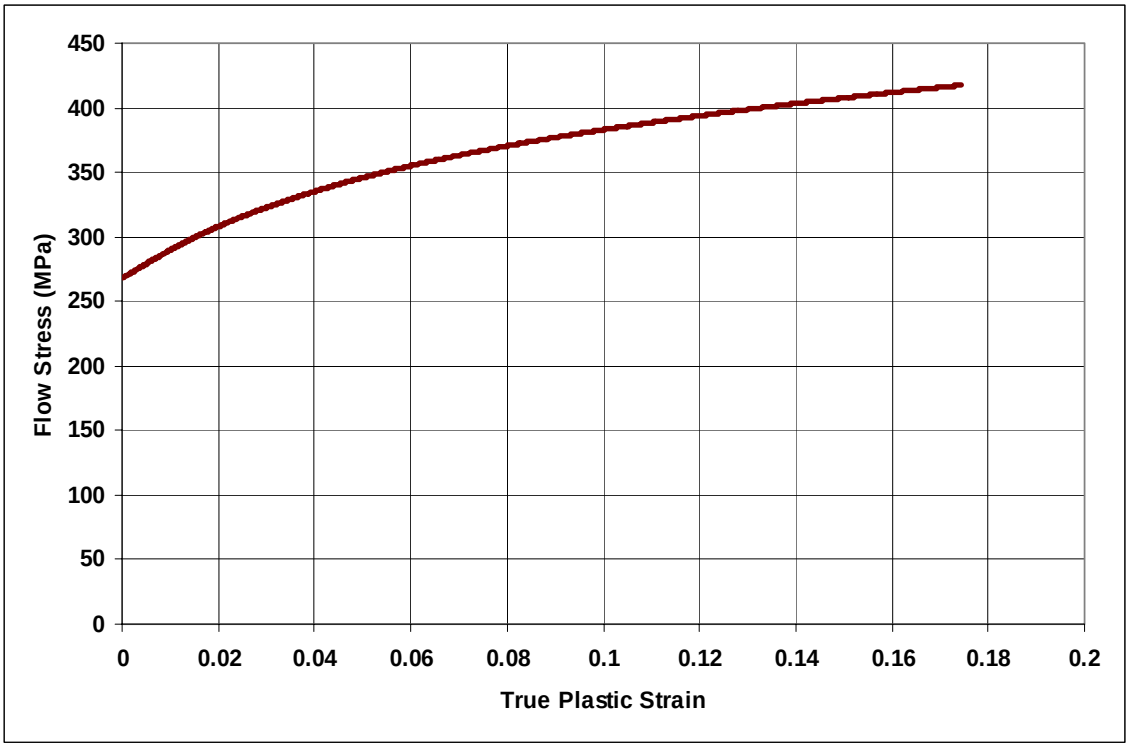

Figure 3.7 Flow curve of ST12

The flow stress at higher strain values can be obtained from the extrapolation of the experimental flow curves by using Ludwick's, Swift's, Voce laws, given in Eqs. (2.17), (2.18), (2.20) respectively.

Both experimental and extrapolated flow curves are shown in Figure 3.8. Voce, Ludwick's and Swift's equations are showing strain hardening behavior. All extrapolated flow curves are compared with the results obtained from the generated computer code and those from the hydraulic bulge test so best extrapolated curve choose to this material.

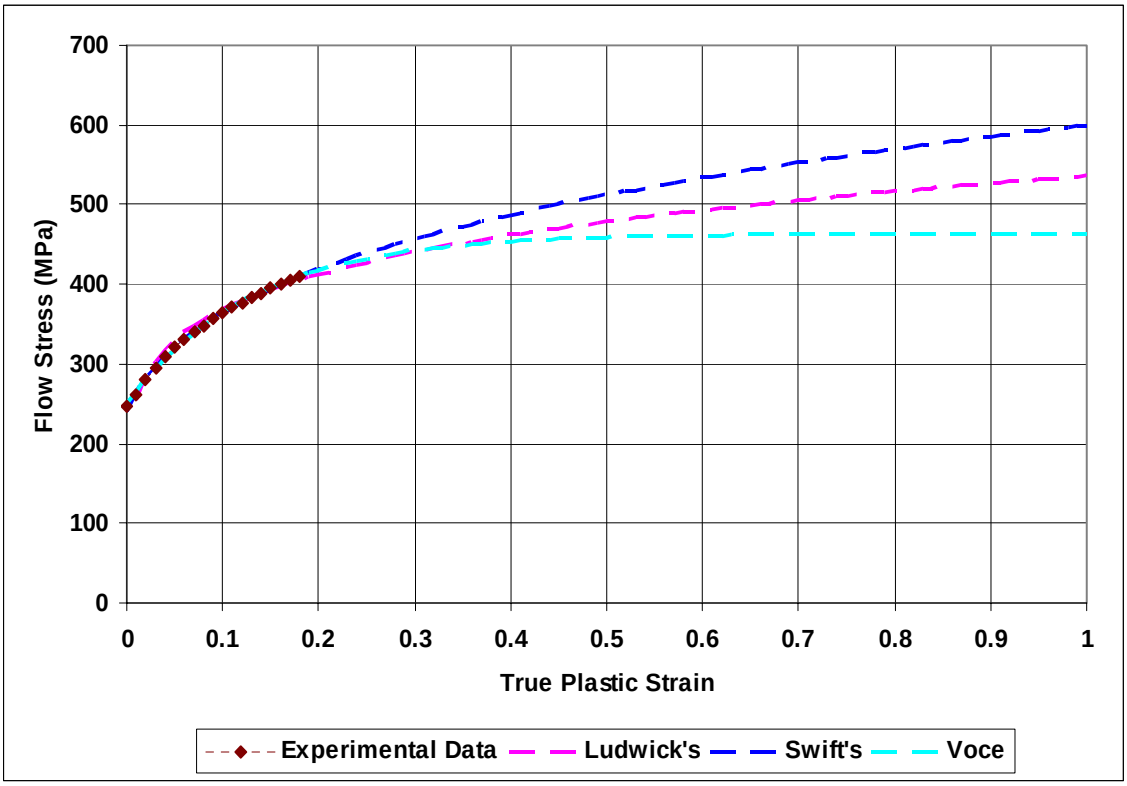

Figure 3.8 Extrapolated flow curve of ST12

The Basics of Strain Calculations for Non-Contact Optical Deformation Measuring System (Gom-Aramis) [32]

With optical measurement techniques (e.g. ARAMIS, ARGUS) coordinates, displacements and strains will be determined only on the surface of objects. This means that the calculation is limited to local strains, which are tangential to the surface.

As additional information perpendicular to the surface is missing, it is not possible to calculate a complete 3D strain tensor (strain values). In this case, the calculation of the thickness change is based on the assumption of volume constancy of the material during loading.

Strain is the measure for the deformation of a line element and can be defined as follows:

$$\lambda = \lim_{l \to 0} \left(\frac{l + \Delta l}{l} \right) \tag{3.2}$$

The stretch ratio λ is the relative elongation of an infinitesimal line element. A strain value ε can be defined as the function of the stretch ratio λ:

The following known functions are frequently used strain measures:

Engineering strain

$$\varepsilon_{eng} = f(\lambda) = \lambda - 1 \tag{3.3}$$

Logarithmic or true strain

$$\varepsilon_{true} = f(\lambda) = \ln(\lambda) \tag{3.4}$$

- Deformation Gradient Tensor Definition

The stretch ratio is defined in the one-dimensional case and the general description of a strain measure. In this section extended to the two-dimensional case.

In order to quantitatively display the deformation of a surface element, the deformation gradient tensor F is introduced. The deformation gradient tensor transforms a line element $\overrightarrow{dX}$ (in reference configuration) into the line element $\overrightarrow{dx}$ (in current configuration). In both cases, the line element connects the same material coordinates. Theoretically, it must be an infinitesimal line element. Translation and strain of a line element figure is shown in Figure 3.9.

Thus, the deformation gradient tensor is defined as:

$$dx = F.dX \tag{3.5}$$

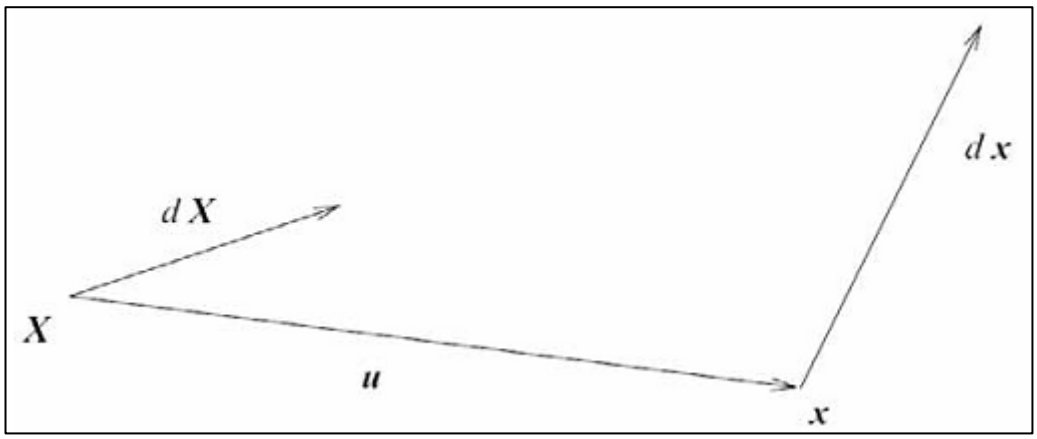

Figure 3.9 Translation (u) and strain of a line element

- Decomposing the Deformation Gradient Tensor

A disadvantage of the deformation gradient tensor is that rotation and stretch are modeled using one matrix only. This can be compensated by splitting the deformation gradient into two tensors: purely rotation matrix and pure stretch tensor. The matrix can be decomposed in two different ways:

Decomposition into rotation R and right stretch tensor U. Mathematically, the deformation gradient tensor is decomposed as follows:

$$F = R.U \tag{3.6}$$

Decomposition into left stretch tensor and rotation. Mathematically, the deformation gradient tensor is decomposed as follows:

$$F = V.R \tag{3.7}$$

- Definition of the x-y Strain Values in 2D

$\varepsilon_x, \varepsilon_y$ and ε_{xy} values can directly be evaluated from the symmetric stretch tensor U with the following form:

$$U = \begin{pmatrix} U_{11} & U_{12} \\ U_{21} & U_{22} \end{pmatrix} = \begin{pmatrix} 1+\varepsilon_x & \varepsilon_{xy} \\ \varepsilon_{xy} & 1+\varepsilon_y \end{pmatrix} \tag{3.8}$$

The strain values $\varepsilon_x, \varepsilon_y$ and ε_{xy} have the disadvantage of being defined depending on the coordinate system used. For the geometrical interpretation of the values ε_{xy} the shear angle γ_{xy} is used. This angle describes the change of an angle in the undeformed state to a new angle in the deformed state.

For large strain values and angles as used in this study, the assumption for small strains from the elastic strain theories must not be used.

$$\gamma_{xy} \neq 2\varepsilon_{xy} \tag{3.9}$$

The definition of the shear angle is shown below:

$$\gamma_{xy} = \gamma_x + \gamma_y \tag{3.10}$$

$$\gamma_x = \arctan(\varepsilon_{xy}/(1+\varepsilon_x)) \tag{3.11}$$

$$\gamma_x = \arctan(\varepsilon_{xy}/(1+\varepsilon_y)) \tag{3.12}$$

The fixed values for γ_x and γ_y show that the orientation of the parallelogram to the coordinate system is fixed. The stretch tensor cannot describe rotations. The coordinate system is defined as x" – y" system (see in Figure 3.10).

- Definition of the 2D Coordinate System and Strain Directions

The deformation gradient tensor F creates a functional connection between the coordinates of the deformed points $P_{v,I}$ and the coordinates of the undeformed points $P_{u,I}$ (I being the index for the different points) and u_i is rigid body translation. The functional connection for each local point is as follows:

$$P_{v,I} = u_i + F.P_{u,I} \tag{3.13}$$

The deformation gradient tensor F=R U can be split into the rotation matrix R and the stretch tensor U. The rotation matrix R describes the rotation of the points and the directions only.

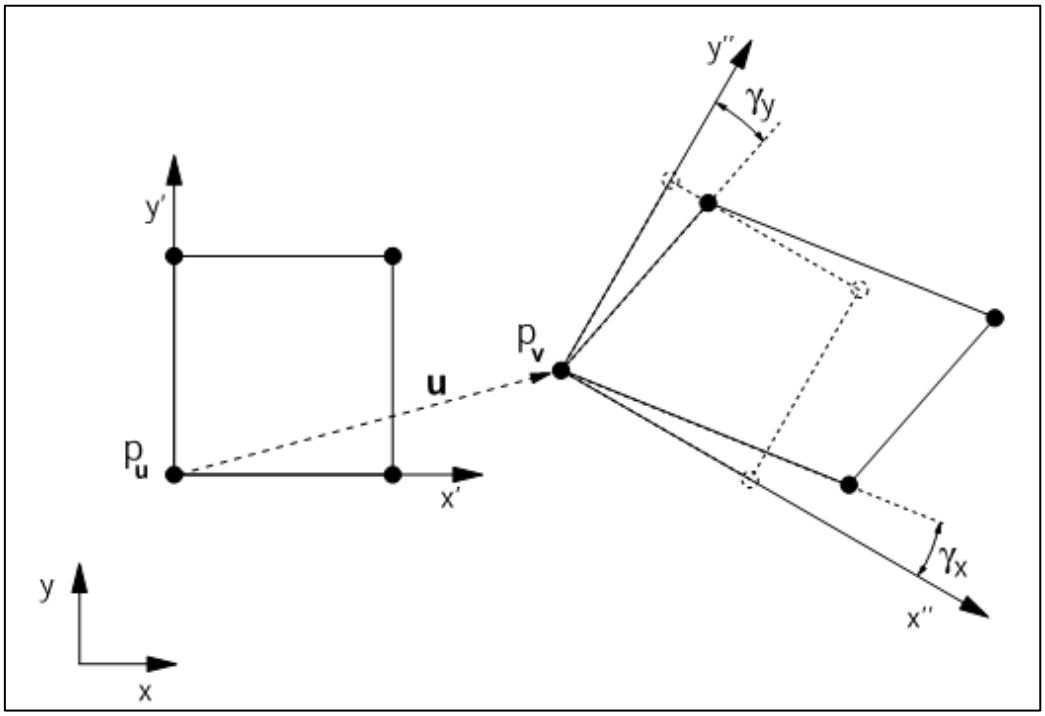

Figure 3.10 Definition of the coordinate system (based on the deformation of a unit square)

Different coordinate systems are used.

x-y: global coordinate system

x'-y': local undeformed coordinate system

x''-y'': local translated and rotated coordinate system

The coordinates of the point are calculated in the global x-y coordinate system. For the 2D discussion, the coordinate system x'-y' is parallel to x-y, but is placed in the undeformed position of the point of interest $P_{u,I}$.

The rotation matrix R defines the rotation from the x'-y' to the x''-y'' system. The coordinate system x''-y'' for the strain calculation is independent from rigid body

movement and rotation. It shows the deformation introduced by the stretch tensor U and defines the direction of the strain values. This leads to:

X'' direction = direction of normal strain x"
Y'' direction = direction of normal strain y"

- Major and Minor Strain Derived From the Deformation Gradient Tensor

The strain measures ε_x and ε_y have the disadvantage of being defined dependent on the coordinate system. This disadvantage can be eliminated by calculating major and minor strain values. The symmetrical matrix U can be transformed to the main diagonal form. The two Eigenvalues ε_1 and ε_2 can be calculated as follows:

$$\varepsilon_{1,2} = \frac{\varepsilon_x + \varepsilon_y}{2} \pm \sqrt{\left(\frac{\varepsilon_x + \varepsilon_y}{2}\right)^2 - \left(\varepsilon_x . \varepsilon_y - \varepsilon_{xy}^2\right)} \qquad (3.14)$$

Based on the larger Eigenvalue, the major strain is determined (ε_1 or φ_1), and based on the smaller Eigenvalue the minor strain (ε_2 or φ_2) is obtained. The corresponding eigenvectors determine the two directions of major and minor strain. The strain values thus determined are independent of the coordinate system and are universally applicable.

If the material thickness with respect to the entire surface is small, it is frequently necessary to deduce the remaining material thickness from the deformation of the surface. As the optical measuring techniques used cannot obtain any data in this dimension, the third principle strain ε_3 can be calculated from major and minor strain ε_1 and ε_2, assuming a constant volume (see in Figure 3.11). The volume constancy can be defined as follows:

$$\varepsilon_1 + \varepsilon_2 + \varepsilon_3 = 0 \qquad (3.15)$$

Or

$$\lambda_1 . \lambda_2 . \lambda_3 = 1 \qquad (3.16)$$

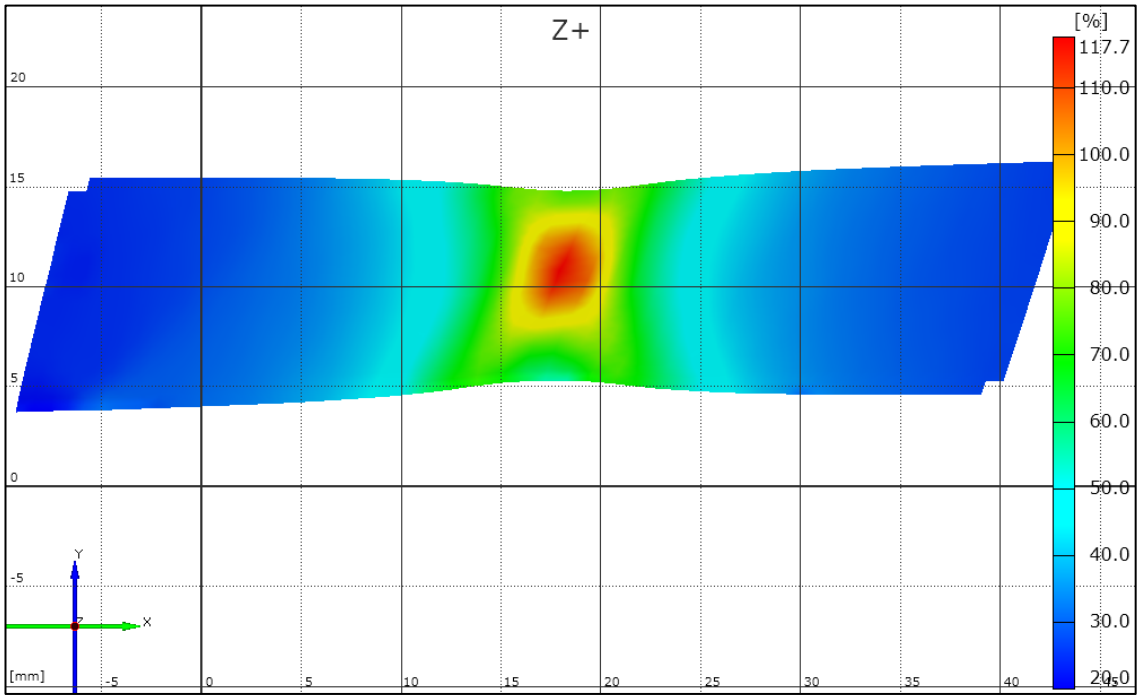

Figure 3.11 Major strain calculation ST12 using by Aramis

Frequently, the effective strains are needed. The effective strains according to von Mises and von Tresca are available. The effective strain according to von Mises results from the following formula:

$$\varepsilon_{von-mises} = \sqrt{\frac{2}{3}\left(\varepsilon_1^2 + \varepsilon_2^2 + \varepsilon_3^2\right)} \tag{3.17}$$

As ε_3 is included in the formula, the effective strain is only valid if the volume constancy is valid. Another formula is:

$$\varepsilon_{von-mises} = \sqrt{\frac{4}{3}\left(\varepsilon_1^2 + \varepsilon_2^2 + \varepsilon_1.\varepsilon_2\right)} \tag{3.18}$$

The effective strain according to von Tresca results from the following formula:

$$\varepsilon_{tresca} = \left|\varepsilon\right|_{\max} \tag{3.19}$$

3.4 Computer Code Methodology

Algorithm is coded in the MATLAB® environment. Gom-Aramis system is arranged to take several pictures at a given constant frequency during the tension test. Defining a reference state, a virtual mesh is attached on the surface of the specimen, which is then distorted as the specimen deforms. Detailed information corresponding to each picture (also called stage) is stored as a corresponding stage file. Deformed coordinates, principal strains, and their directions, forming the content of this file, are computed for each *node* of the mesh. Naming the node which attains highest strains as the *highest-strained node*, the series of mesh nodes including this node and forming the cross-section is named as *the highest-strained section (HSS)*.

Considering a virtual cut through the HSS, at each stage *j*, the integral of tractions over *segments* forming the HSS, equals the corresponding experimental tensile force, $F_{tension}^{j}$:

$$F_{tension}^{j} = \sum F_{segment}^{j} \tag{3.20}$$

In this equation the force on each segment is computed using the following formula

$$F_{segment}^{j} = \left(\frac{\sigma_1 + \sigma_2}{2} \cos\alpha + \frac{\tau_1 + \tau_2}{2} \sin\alpha \right) \frac{t_1 + t_2}{2} L \tag{3.21}$$

Where the indices 1 and 2 refer the fist and the second node (i.e., end nodes) of the segment, respectively. Normal σ and shear τ traction are obtained by transform-ing the principal stresses σ on the plane of the segment. Thickness *t* at each node is computed using strain measurements. α is the angle between tension direction and the normal vector of the segment. Finally, *L* is the length of the segment. Values for α, *t* and *L* are obtained from Gom-Aramis measurements. Utilizing the principle strains (measured by Gom-Aramis) and the equivalent total plastic strain, $\bar{\varepsilon} = \sqrt{2/3\ \varepsilon_{ij}\varepsilon_{ij}}$, principal-stress-deviator, s, is computed from Hencky' s stress-strain relation:

$$s = \frac{2}{3}\frac{Y}{\bar{\varepsilon}}\varepsilon \tag{3.22}$$

Assuming the stress component in the thickness direction is zero, components of the principal stress σ could be computed easily. The unknown value of the yield stress *Y* in this equation is obtained at each stage and for each node of the HSS using the following approach:

Considering the highest-strained node, equivalent total plastic strain values at each stage forms a list of values for the equivalent total plastic strain, $\bar{\varepsilon}$. Flow curve of the material delivers a corresponding list of the yield stresses Y_i. At a stage it is possible that, a node of the HSS has equivalent total plastic strain value $\bar{\varepsilon}$, falling between two consecutive values $\bar{\varepsilon}_i$ and $\bar{\varepsilon}_{i+1}$ of the strain list. In this case the corresponding value *Y* of the yield stress is computed using the following formula

$$Y = \left(\frac{\bar{\varepsilon}_{i+1} - \bar{\varepsilon}}{\bar{\varepsilon}_{i+1} - \bar{\varepsilon}_i}\right) Y_i + \left(\frac{\bar{\varepsilon} - \bar{\varepsilon}_i}{\bar{\varepsilon}_{i+1} - \bar{\varepsilon}_i}\right) Y_{i+1} \tag{3.23}$$

Using the given derivation from Eq. 3.21 to Eq. 3.23, force balance Eq. 3.20 at each stage, result in an equation in the form of a linear combination of unknown yield stress values Y_i multiplied by computable multipliers (values coming from Gom-Aramis measurements), being equal to the measured tensile force. Considering the whole set of such equations, for all measurement stages, one obtains a set of equations in the following form

$$\begin{bmatrix} Square \\ Multiplier \\ Matrix \end{bmatrix} \{Y_j\} = \{F^j_{tension}\} \tag{3.24}$$

Solving the equation system gives directly the yield stress values Y_j corresponding to total plastic strain values $\bar{\varepsilon}_i$.

It is not necessary that the initial stage for the above computation is the reference (zero load) state. Any stage could be selected as the beginning stage as far as the synchronisation between the two measurements done by Gom-Aramis and the tensile testing machine (being the tensile forces) is guaranteed. This is easily achieved by matching up the point of rupture in these two measurements.

All results are recorded in text files, approximately 150 files, for each stage. After the code calculated true stress, true strain values are evaluated according formulations using the data provided by the text files. Algorithm flow chart is represented in Figure 3.12.

Inputs of the code are;

- **Thickness of the Material:** Initial thickness of the material,
- **Stage of the Initial Yield:** The material starts yielding at this stage,
- **Measured Force:** Tensile testing machine is given that delivers this value,
- **Name Convention:** Name of the text files are input. Sample name convention is "ST12_1_i.txt" where "i" varies from 1 o 150 approximately,
- **Major and Minor Principal Strains:** Aramis calculated that these values for each stage,
- **Major and Minor Principal Strains Directions:** Aramis calculated that these values for each stage,
- **Deformed and Undeformed Coordinates:** Aramis is given that value for each stage and for each node.

Code gives the following outputs.

- **Instantaneous Thickness of the Material:** Instantaneous thickness of the material for each stage,
- **Line Integral:** All segment integral is calculated,
- **All Unit Vector:** Common x, y, z direction unit vector are calculated,

- **Plastic Strain:** This result is calculated using by equivalent plastic strain result,
- **Flow Stress:** This result is calculated by measured force and multiplier matrix.

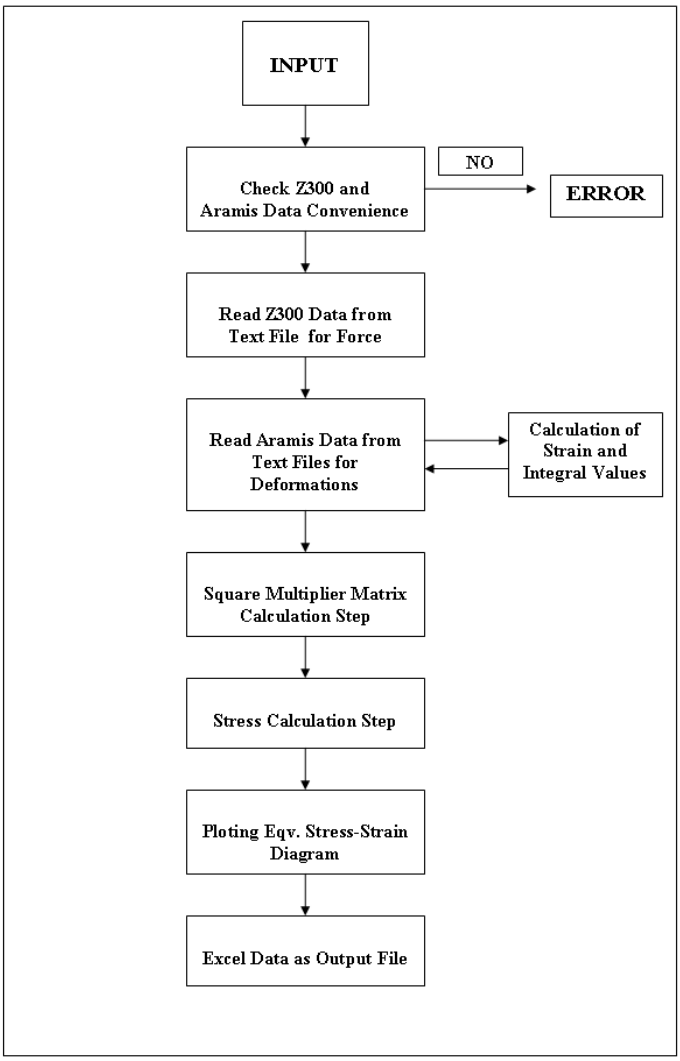

Figure 3.12 Flow chart of developed computer code

Developed algorithm is tested using three tensile tests. The code results are very close to each other so, one of them is chosen in the results. Other repetitions are given in the APPENDIX A. Conventional flow curve from tensile testing machine measurements, (using precise tangible extensometers), flow curve using the proposed approach (used by computer code) and, extrapolated flow curves is shown in Figure 3.13.

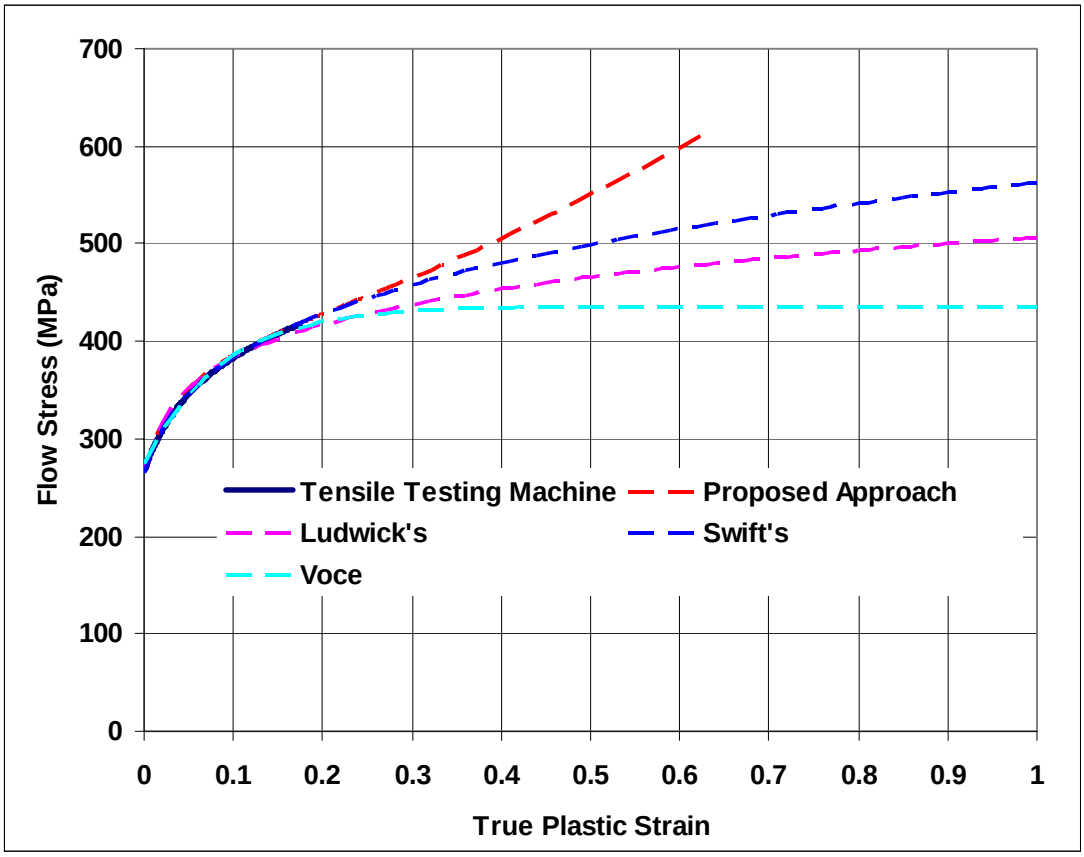

Figure 3.13 Flow curves of ST12 evaluated by various methods.

3.5 Finite Element Simulation

Modeling of the experiments by using finite element analysis is performed as a next step. Finite element simulation is done using commercial finite element program MSC. Marc®. Tensile testing machine (Zwick Z300E) measured forces and finite element simulation program resulted forces are compared in Figure 3.14. This comparison shows that the obtained flow curve using the proposed approach is true because the measured and finite element simulation results overlap.

Finite element simulation is done by using 3D shell elements. Material data is selected according to the proposed approach flow curve and elastic plastic material behavior. Full specimen geometry is used. The other parameters and details of FEM simulation are tabulated in Table 3.1.

Table 3.1 Parameters used in FEM simulations

Steel ST12	Analysis Options	FEM program	Marc Mentat 2007
		Iteration Method	Full Newton Raphson
		Workpiece Material Type	Elastic - Plastic
		Convergence Ratio	Residual Force: 0.05
		Number of Elements	5000-6000
		Number of Steps	300-400
		Remeshing	No
		Material	Proposed Flow Curve
		Modulus of Elasticity	210000 MPa
		Poisson's Ratio	0.3

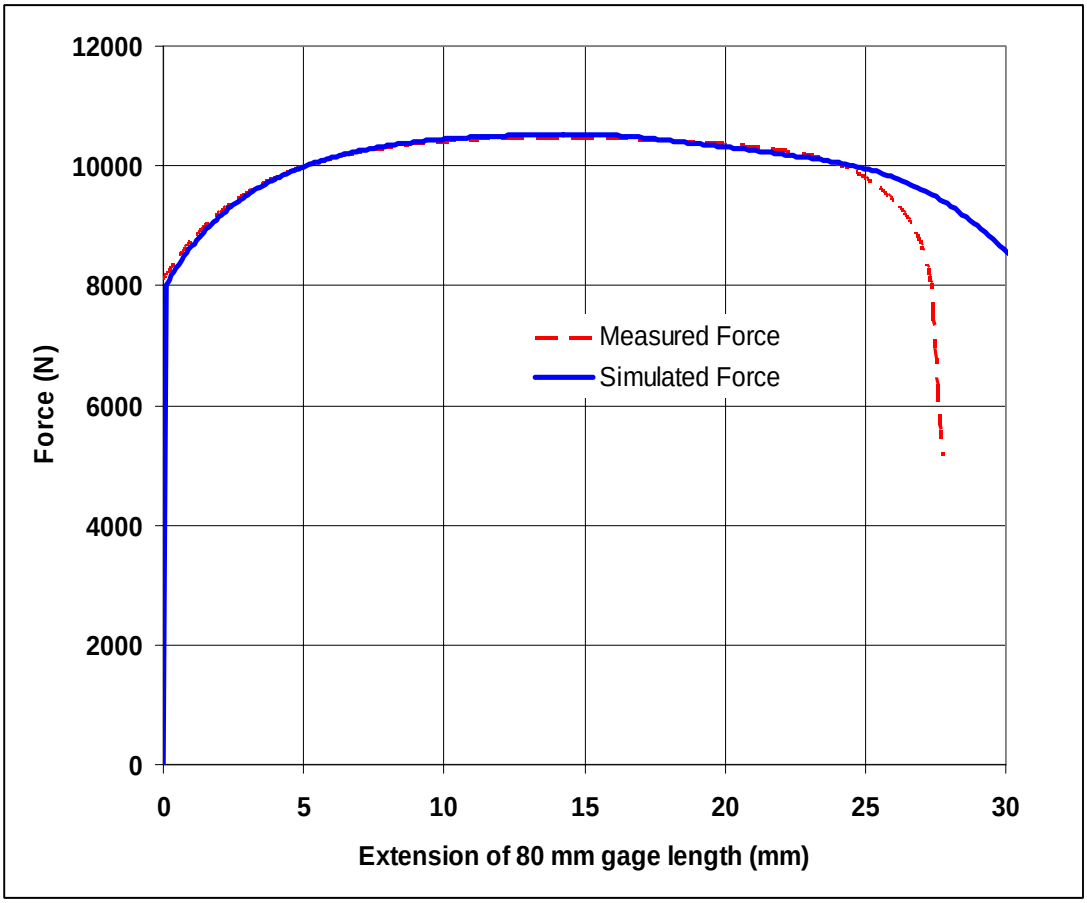

Figure 3.14 Simulation and experimental results compared

Simulation model meshes and total equivalent plastic strain results are given in Figure 3.15. Quad meshes are used in simulation.

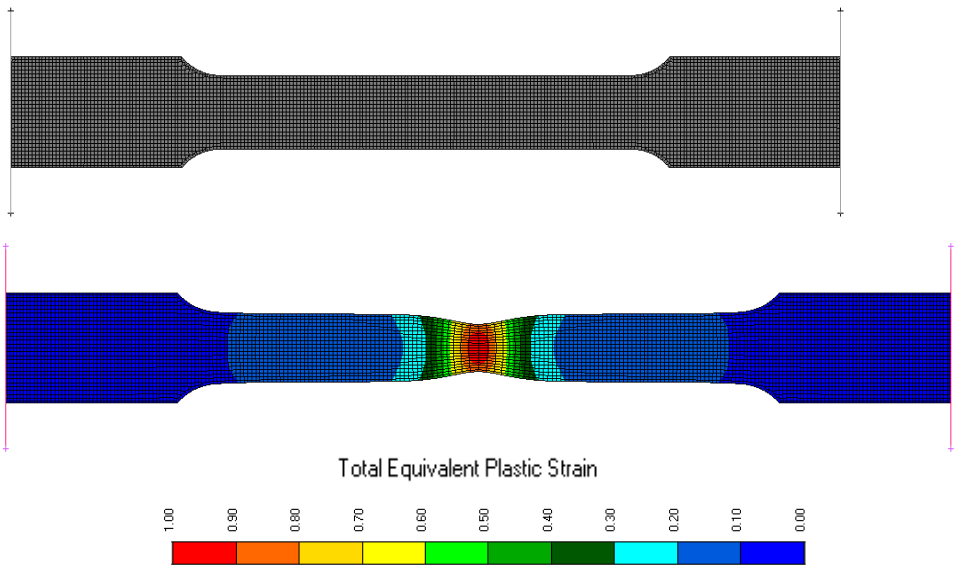

Figure 3.15 Simulation of the tension test using the flow curve obtained by the introduced method

Finite element simulation calculated total equivalent plastic strain results and Aramis measured total equivalent plastic strain results are compared in Figure3.16.

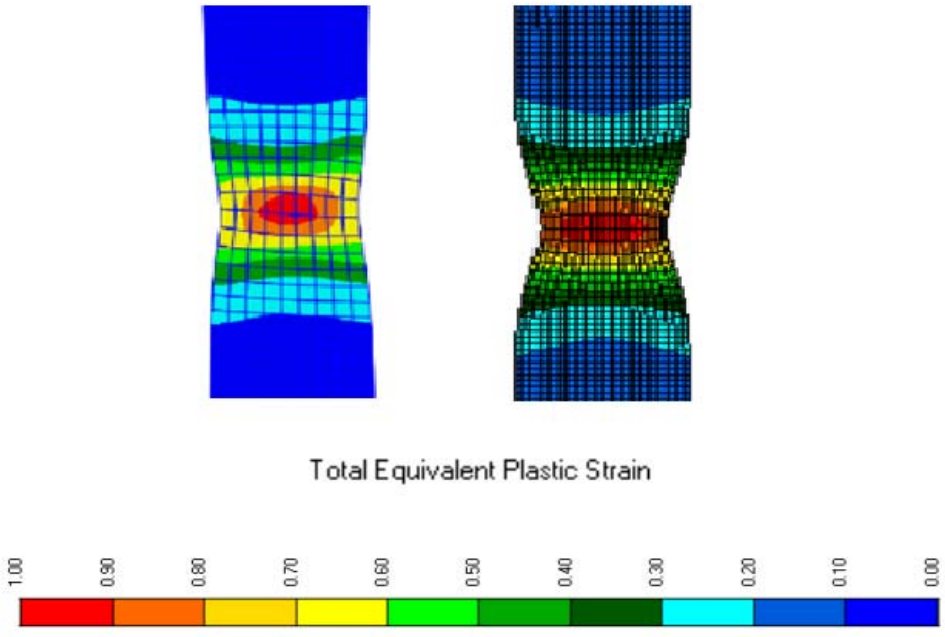

Figure 3.16 Aramis measured equivalent plastic strain and Fem resulted equivalent plastic strain, respectively

3.6 Comparison with Hydraulic Bulge Test Result

In this chapter, computer code result (used optical data), tensile testing machine result and hydraulic bulge test result are compared. Hydraulic bulge test experimental procedure and how to find flow curve using by Matlab® code are explained.

Experimental Procedure

HBT tests are carried out in a Zwick//Roell BUP 600 (60 ton) computer controlled hydraulic test machine at room temperature. Upper and lower dies have 160mm diameter drawbead to prevent material flow in clamping region. In this manner, the sheet has no draw-in and it is only stretched by pressurized fluid. Complete HBT system is shown in Figure 3.17.

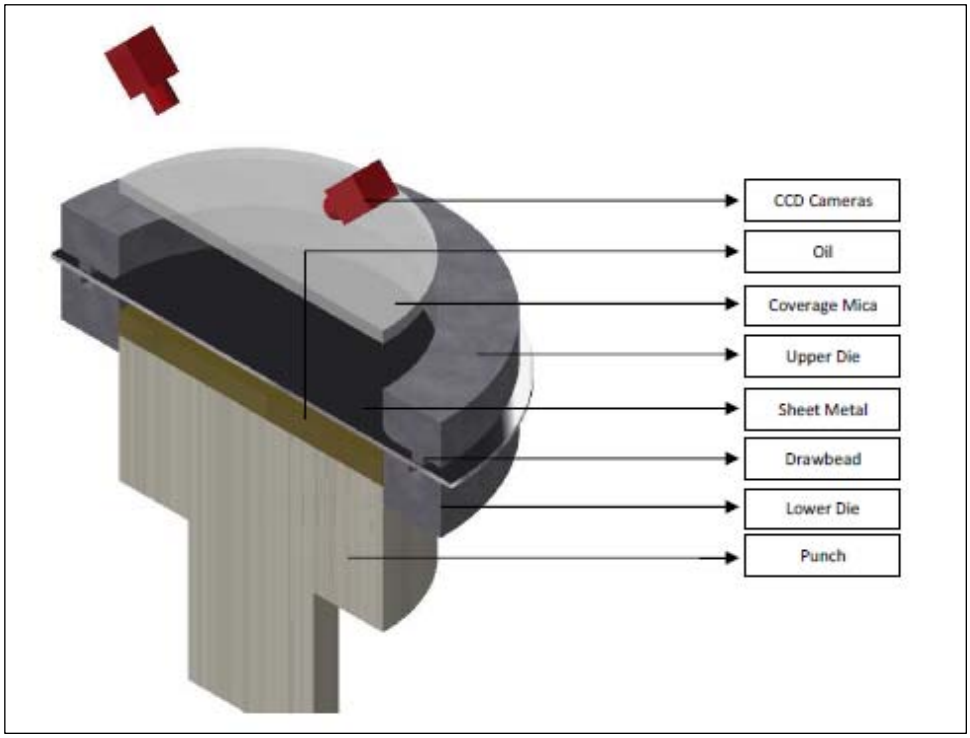

Figure 3.17 Experimental setup with hydraulic bulge test

Commercial Aramis digital image correlation (DIC) systems from GOM and the same systems are used to measure the displacement field during loading. Two high-resolution cameras (2358 * 1728 pixels) with Titanar 65mmf/2.8 lenses are used

[32]. The cameras are mounted on an upper BUP 600 machine and arranged so that upper face of the specimens is visible to both cameras simultaneously. A complete system calibration is run before each experiment to ensure accurate results. A plate with a pre-defined pattern of circular dots is moved around in the measurement area while both cameras acquired several synchronized calibration images.

Measurements and Computer Code

HBT are repeated three times to ensure reparability. The results are very close to each other so, only one of them is chosen in test results. Experimental output has been taken as a bulge force, time and optical measure strain values. True stress and true strain curve is generated as proposed in [37] computer code.

Measurement procedure is described below: Lower die is pushed with high viscosity fluid. A transparent cover is placed between upper die and high resolution CCD cameras since oil spouts as the material bursts. After the cover is placed, led lamps is set to taking account of prevent reflection. Then the deformation is recorded up to fracture stage. For a simple test, approximately 450 photos are recorded. Simultaneously, BUP 600 test machine results are recorded with 0.01-second time interval.

3D optical strain measurement system is used for measurement side of the deformation. During test, 2 CCD cameras with at 20 Hz are used.

Different nodes section over the crack region and crack region are taken to collect data (see in Figure 3.18). For each node and each stages, displacements along x, y and z directions are obtained. All results are recorded in a text files, approximately 450 files, for each stage. After the code calculates true stress, true strain values according the analytical and numerical formulations are obtained using the data in the text files.

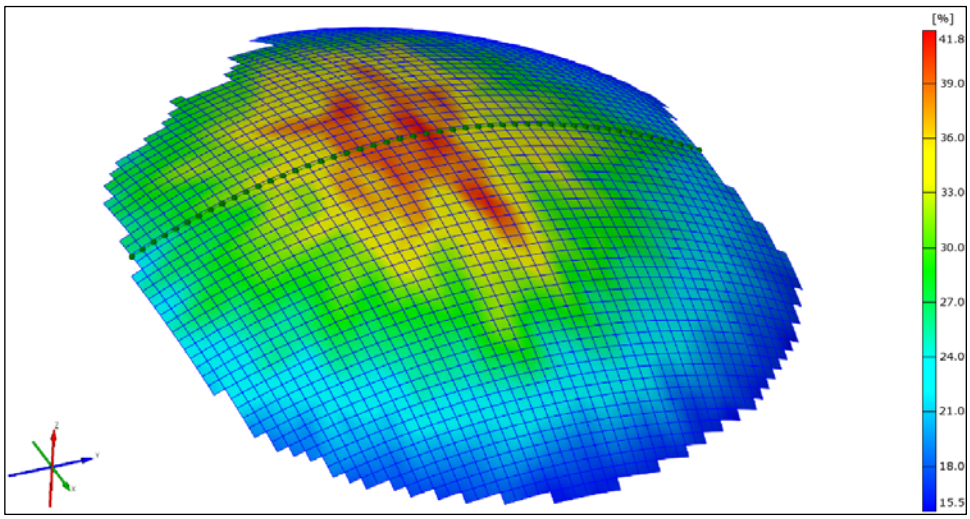

Figure 3.18 Aramis results with a section

Inputs of the code are;

- **Thickness of the material:** Initial thickness of the material,
- **Fracture time of the metal:** Fracture time of the sheet metal that is read from BUP600 output data and inputted manually,
- **Critical node:** Critical node number is given to specify the thinnest portion of the material just before the fracture stage,
- **Name convention:** Name of the text files is inputted. Sample name convention is "ST12_1_i.txt" where "i" varies from 1 o 450 approximately.

Code gives the following outputs.

- **Thickness of the material:** Instantaneous thickness of the material for each stage,
- **Pressure:** Instantaneous pressure of BUP600,
- **Analytical stresses:** Stresses based on Hill and Panknin theorems are taken as output,
- **Analytical thickness:** Instantaneous thickness based on Kruglov, Panknin and Chakrabarty's theorems.
- **Strain:** Kruglov strain values based on Hill and Panknin's methods. Additionally, Hill's and Chakrabarty's strains,

- **Stress:** Stress values for each stage based on $\sigma = \frac{p.r}{2.t}$ theorem where p is the pressure while r is instantaneous bulge radius and t is the thickness of the material at the dome.
- **Bulge radius:** Bulge radiuses based on analytical models and two different special cases, which are usage of sectional data over the crack region and the nodes, those have descending order by means of z-displacements.

$$\sigma = \frac{p.r}{2.t} \tag{3.25}$$

Hill's analytical bulge radius [35]

$$\rho_H = \frac{r_c{}^2 + h_d{}^2}{2.h_d} \tag{3.26}$$

Panknin's analytical bulge radius [36]

$$\rho_P = \frac{\left(r_c + r_f\right)^2 + h_d{}^2 - 2.r_f h_d}{2.h_d} \tag{3.27}$$

Where;

- t : Instantaneous thickness (mm)
- t_0 : Initial thickness of the sheet (mm)
- ρ : Instantaneous bulge radius (mm)
- r_c : Radius of hydraulic piston (mm)
- r_f : Die radius (mm)
- h_d : Instantaneous height of dome (mm)
- p : Pressure (N/mm^2)

As a First method, analytical calculations are based on Hill [35] and Panknin [36]. Analytical methods to calculate bulge radius use both radius of pressuring piston and

the instantaneous height of peak point. Developed code determines the most critical node, which has the highest z-displacement for each step and calculated instantaneous radius of bulged material.

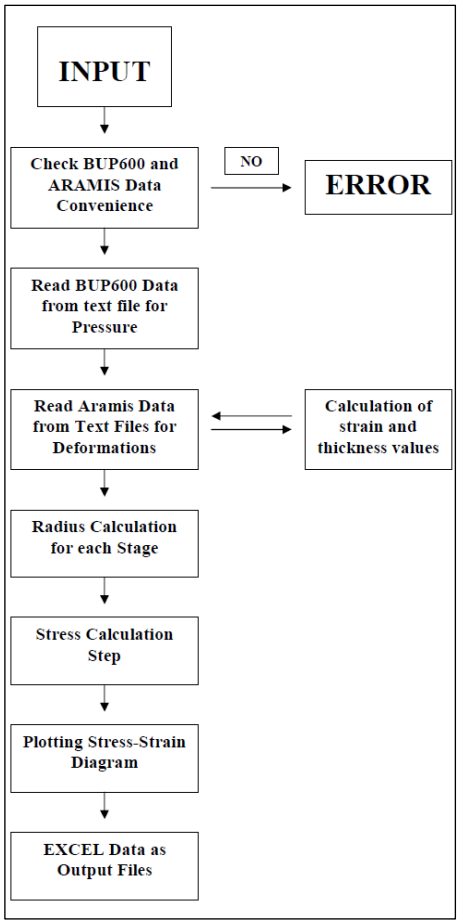

Figure 3.19 Flow chart of developed MATLAB code [37]

As for a Second method, bulge radius are calculated using nodal coordinates. For n number of nodes, which are placed on the section, radius is calculated for $\frac{n}{2}$ number of nodes. Results for 5, 10, 15 and 25 number of nodes those are placed on section are compared.

Third method is the point cloud method. The code determines the maximum nodal displacement and categorizes the nodes in a descending order. So, the radius calculation is based on the n number of nodes, which have maximum z-displacement (Figure 3.20).

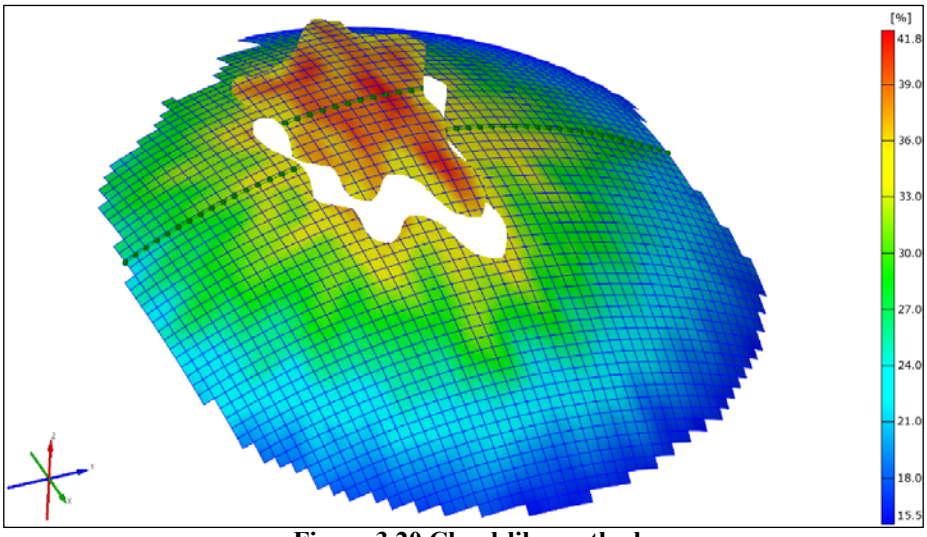

Figure 3.20 Cloud-like method

Finally, GOM-ARAMIS software is used in order to get bulge radius for each step. Aramis software calculates instantaneous sphere radius (Figure 3.21). In this method, all the nodes are used to calculate bulge radius, which is used to obtain stress.

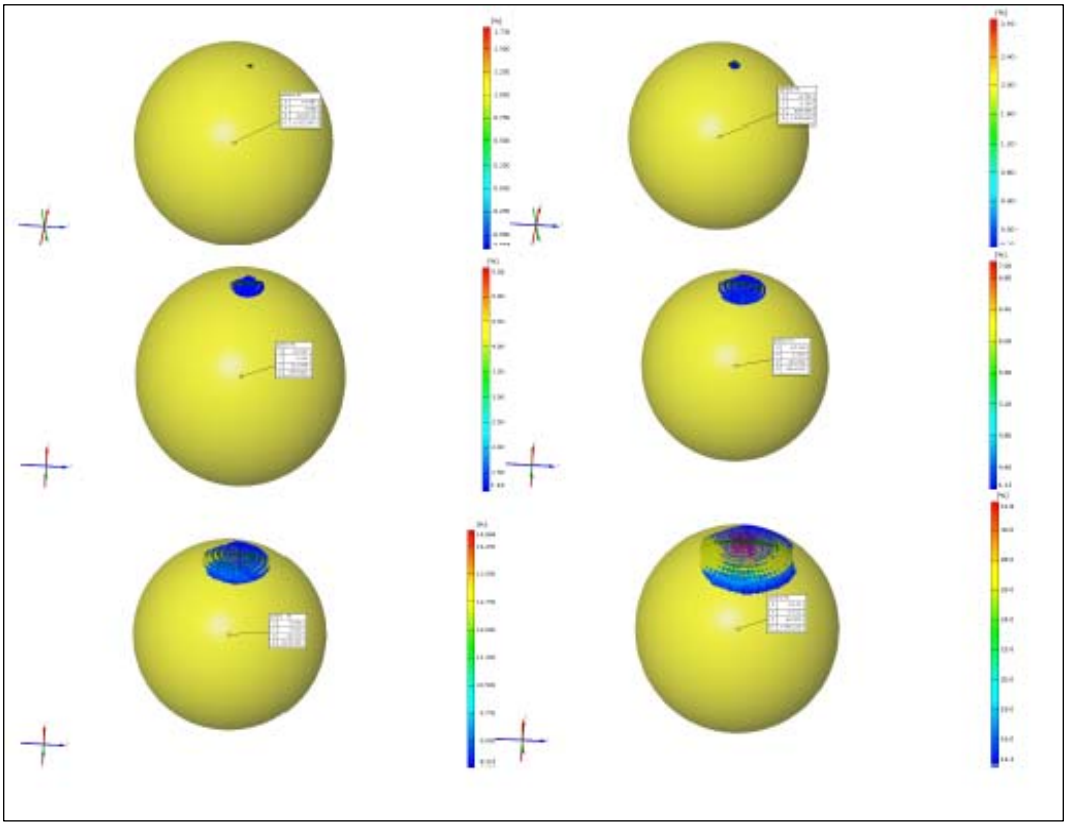

Figure 3.21 Some steps of Aramis best fit sphere

Strain calculations are performed using Aramis output data. Deformed and undeformed coordinates of nodes in 3D space with thickness reduction are calculated by Aramis software.

Additionally, analytical methods are also used to obtain thickness and thickness strains using following formulas.

Hill's dome thickness

$$t = t_0 \left[\frac{1}{1 + \left(\frac{h_d}{r_c} \right)^2} \right]^2 \quad [38] \tag{3.28}$$

Chakrabarty's and Alexander's dome thickness

$$t = t_0 \left[\frac{1}{1 + \left(\frac{h_d}{r_c} \right)^2} \right]^{2-n} \quad [39] \tag{3.29}$$

Kruglov's dome thickness based on Hill's approach

$$t = t_0 \left[\frac{\frac{r_c}{\rho_H}}{\sin^{-1}\left(\frac{r_c}{\rho_H} \right)} \right]^2 \quad [40] \tag{3.30}$$

Kruglov's dome thickness based on Panknin's approach

$$t = t_0 \left[\frac{\frac{r_c}{\rho_P}}{\sin^{-1}\left(\frac{r_c}{\rho_P} \right)} \right]^2 \tag{3.31}$$

- ε_z : Thickness strain
- t_r : Instantaneous thickness reduction
- ρ_H : Hill's bulge radius
- ρ_P : Panknin's bulge radius
- n : Material hardening exponent

Hydraulic bulge test, tensile test and, proposed approach results are shown in Figure 3.22.

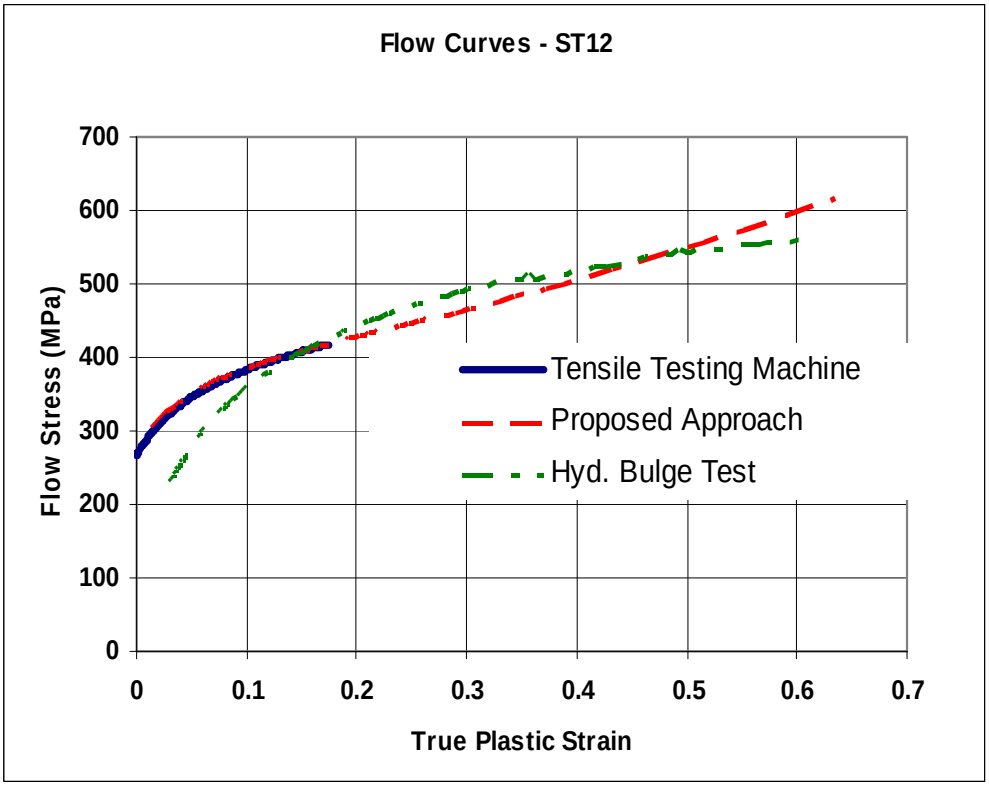

Figure 3.22 Flow curves of ST12 evaluated by various methods

CHAPTER 4

CASE STUDY

4.1 Introduction

In this chapter, flow curve of material St4 will be determined. St4 is supplied from ORS Bearing Company (Ankara, Turkey). First, the material flow curve is obtained by using tensile test machine and optical strain measurement system. Then the strain results are given computer code so the large strain flow curve is found. Finally, the results are compared the hydraulic bulge test results. The modelling of these experiments is explained and the conclusions on the success of large strain flow curve are presented. This chapter is written the same order and same methodology like the Chapter 3. Thus, only experimental and, numerical results are given in this chapter.

4.2 Examination of St4 Steel

In the forth-coming sections, flow curve of the St4 is obtained using the proposed approach. Firstly tensile test results are given. Secondly, computer code results compared with tensile test results. Thirdly, tensile testing machine measured force and, finite element analysis simulated force results are compared. Finally, hydraulic bulge test compared with other results. Thus, flow curve of St4 will be determined using generated computer code.

The composition of the St4 (EN 10130) steel employed in this research is 0.027C, 0.172Mn, 0.009P, 0.008S, 0.003Si, 0.033Al, all numbers are given in mass fraction (%).

4.2.1 Tensile Testing Machine Measurements

Tensile test are repeated three times to ensure repeatability. The results are very closely each other so, one of them is chosen in the test results. This result is used all progress. Other repetitions are given in the APPENDIX A. Experimental output has been taken as a force displacement curve, saved by the testing machine in ASCII format. Force and displacement curve is drawn by using the program Microsoft Excel (Figure 4.1).

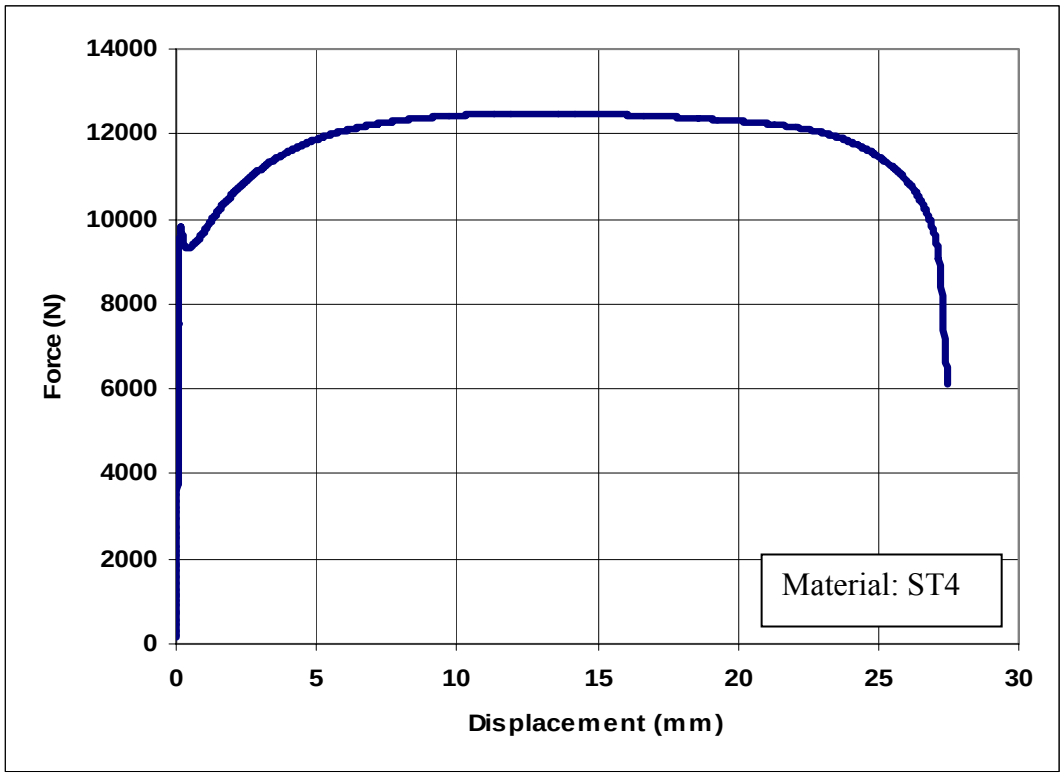

Figure 4.1 Tension test force displacement curve

Force displacement data can easily be converted to engineering stress – engineering strain data with the help of Eqs. (2.1), (2.2) and to true stress- true strain data with the helps of Eqs. (2.5), (2.7). Maximum point on engineering stress – strain curve gives the point where the necking starts and the ultimate tensile strength, σ_{UTS} as shown in Figure 4.2.

For the St4 specimen, ultimate tensile strength can be taken as σ_{UTS} =343 MPa, and necking strain as $\varepsilon_{eng}^{necking}$ =0.19

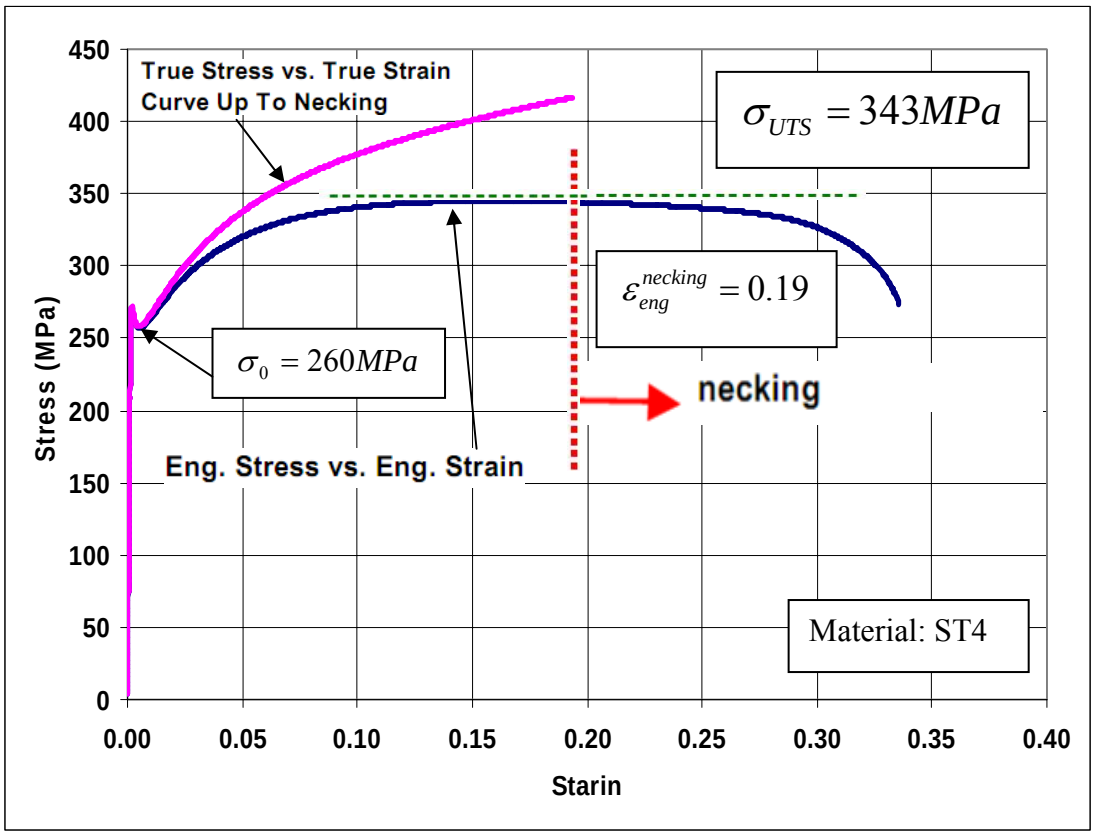

Figure 4.2 Stress and strain curve of material ST4 obtained from tensile test

Material response is clear the yield point region; therefore, 0.2 % offset strain method is not used to define the yield stress for this material. It is shown to be $\sigma_0 = 260MPa$ on Figure 4.2.

The flow curve can be obtained by plotting true stress values against corresponding equivalent true plastic strain values determined by the Eq. (3.1).

Figure 4.3 shows the flow curve of St4 obtained from tension test without any extrapolation.

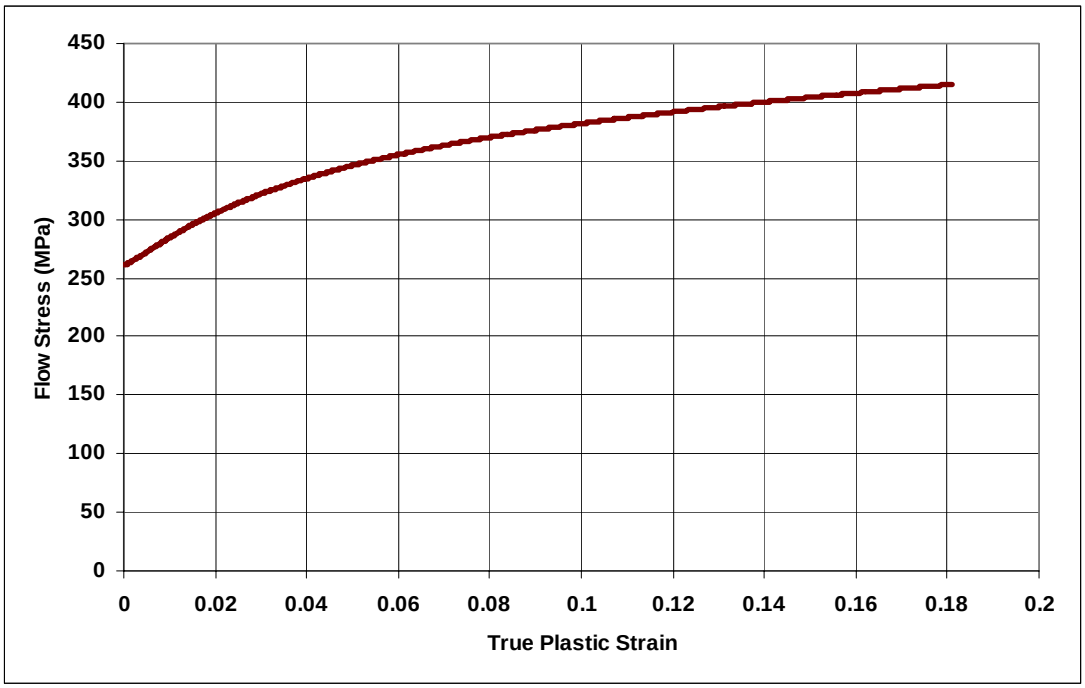

Figure 4.3 Flow curve of ST4

The flow stress higher strain values can be obtained from the extrapolation of the experimental flow curves by using Ludwick's, Swift's, Voce laws, given in Eqs. (2.17), (2.18), (2.20) respectively.

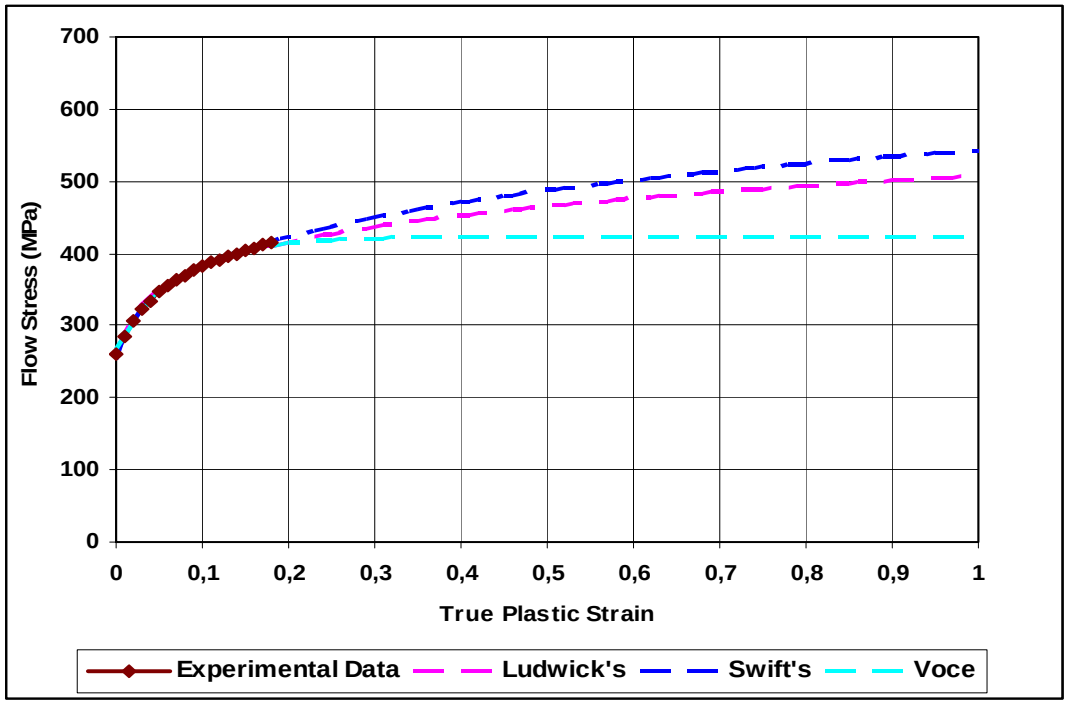

Figure 4.4 Extrapolated flow curve of ST4

Both experimental and extrapolated flow curves are shown in Figure 4.4. Voce Ludwick's and Swift's equations are showing strain hardening behavior. All extrapolated flow curves use to compare by generated computer code result and hydraulic bulge test result so best extrapolated curve choose to this material.

4.2.2 Generated Computer Code Result

Computer code are calculated using by tree tensile testing result. The code results are very closely each other so, one of them is chosen in the results. Other repetitions are given in the APPENDIX A. Tensile testing machine flow curve (using precise tangible extensometers), proposed approach flow curve (used by computer code) and, extrapolated flow curve is shown in Figure 4.5.

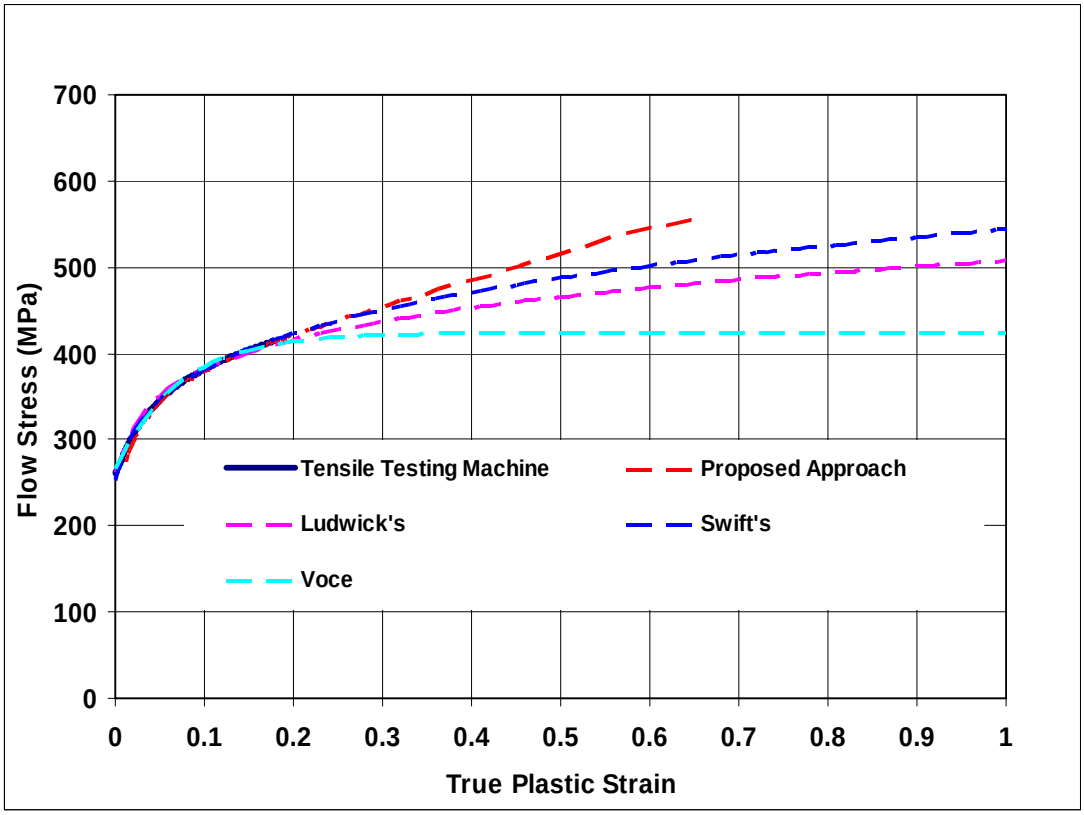

Figure 4.5 Flow curves of ST4 evaluated by various methods

4.2.3 Finite Element Simulation Result

Finite element simulation is done by using 3D shell elements. Material data is selected according to the proposed approach flow curve and elastic plastic material behavior. Full specimen geometry is used. Another parameters and details of FEM simulation are tabulated in Table 4.1.

Table 4.1 Parameters used in FEM simulations

Steel ST4	Analysis Options	FEM program	Marc Mentat 2007
		Iteration Method	Full Newton Raphson
		Workpiece Material Type	Elastic - Plastic
		Convergence Ratio	Residual Force: 0.05
		Number of Elements	5000-6000
		Number of Steps	300-400
		Remeshing	No
		Material	Proposed Flow Curve
		Modulus of Elasticity	210000 MPa
		Poisson's Ratio	0.3

Tensile testing machine (Zwick Z300E) measured forces and finite element simulation program resulted forces are compared in Figure 4.6.

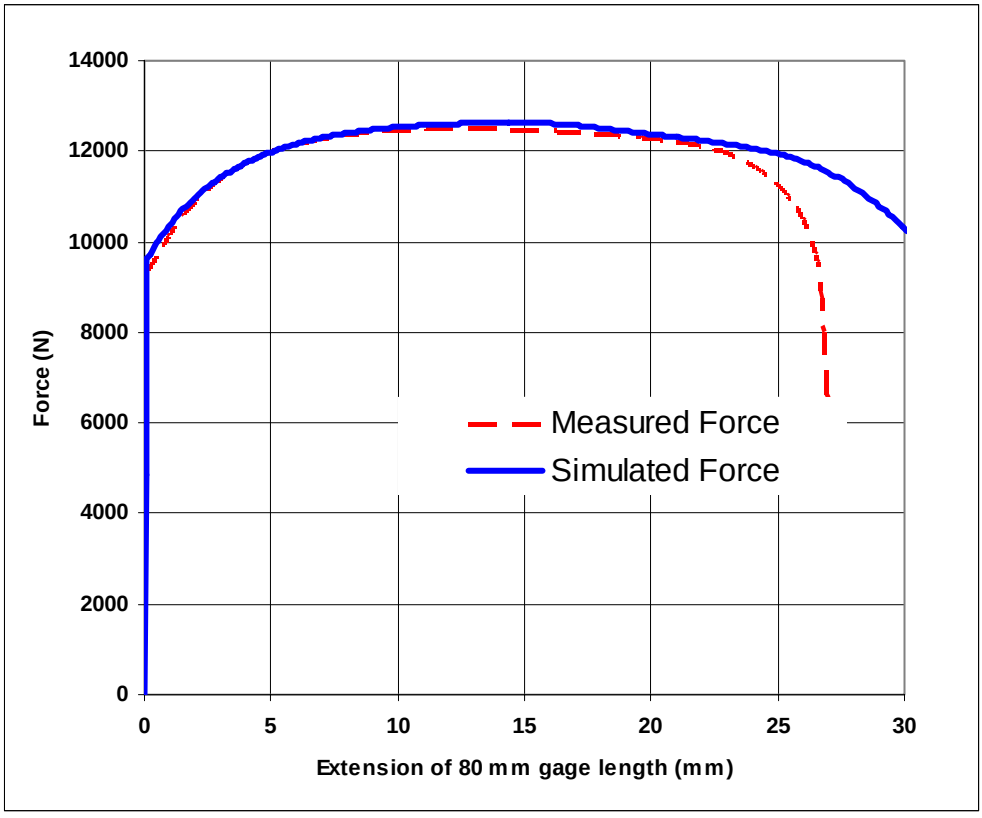

Figure 4.6 Simulation and experimental results compared

Simulation model meshes and total equivalent plastic strain results are given in Figure 4.7. Quad meshes are used in simulation.

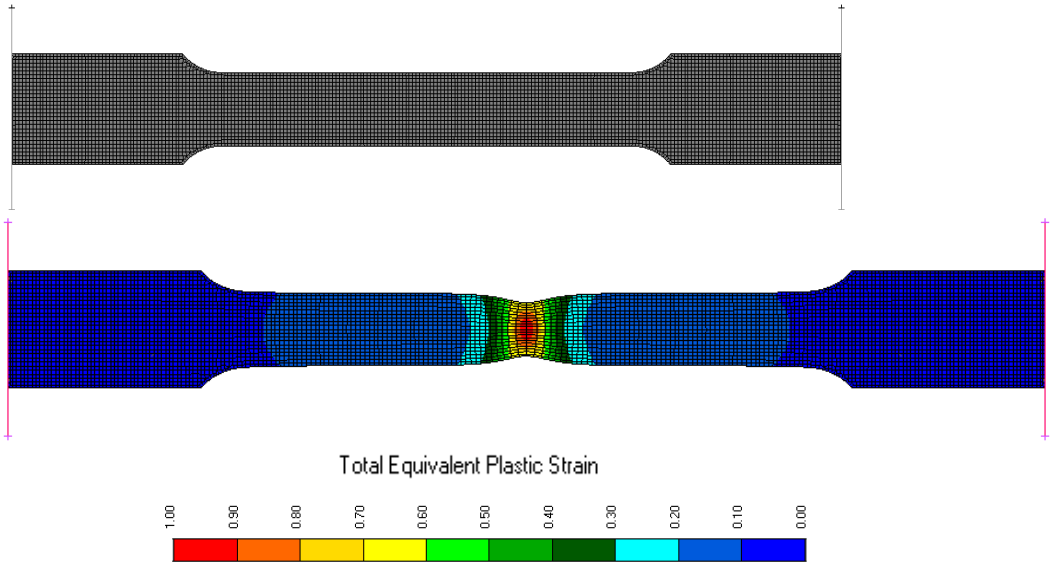

Figure 4.7 Simulation of the tension test using the flow curve obtained by the introduced method

Finite element simulation calculated total equivalent plastic strain results and Aramis measured total equivalent plastic strain results are compared in Figure 4.8.

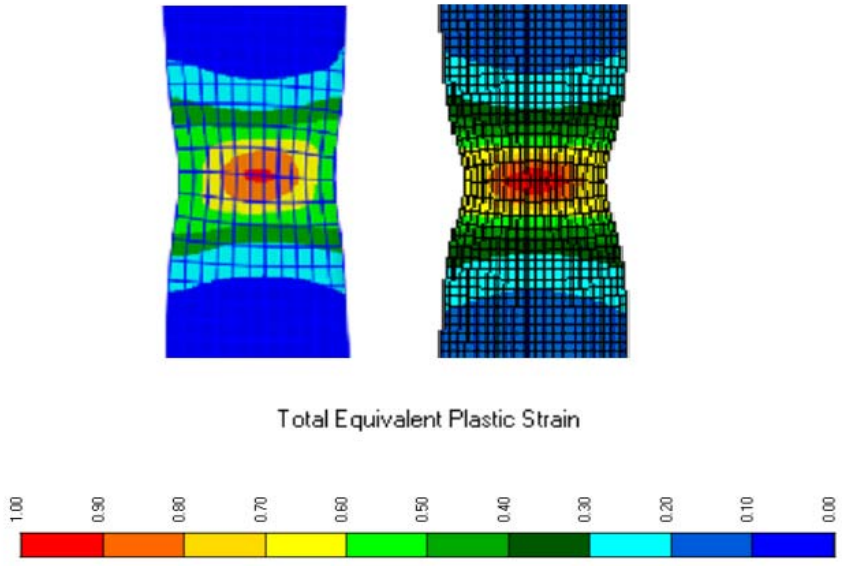

Figure 4.8 Aramis measured equivalent plastic strain and Fem resulted equivalent plastic strain, respectively

4.2.4 Comparison with Hydraulic Bulge Test Result

Hydraulic bulge test, tensile test and, proposed approach result is shown in Figure 4.9.

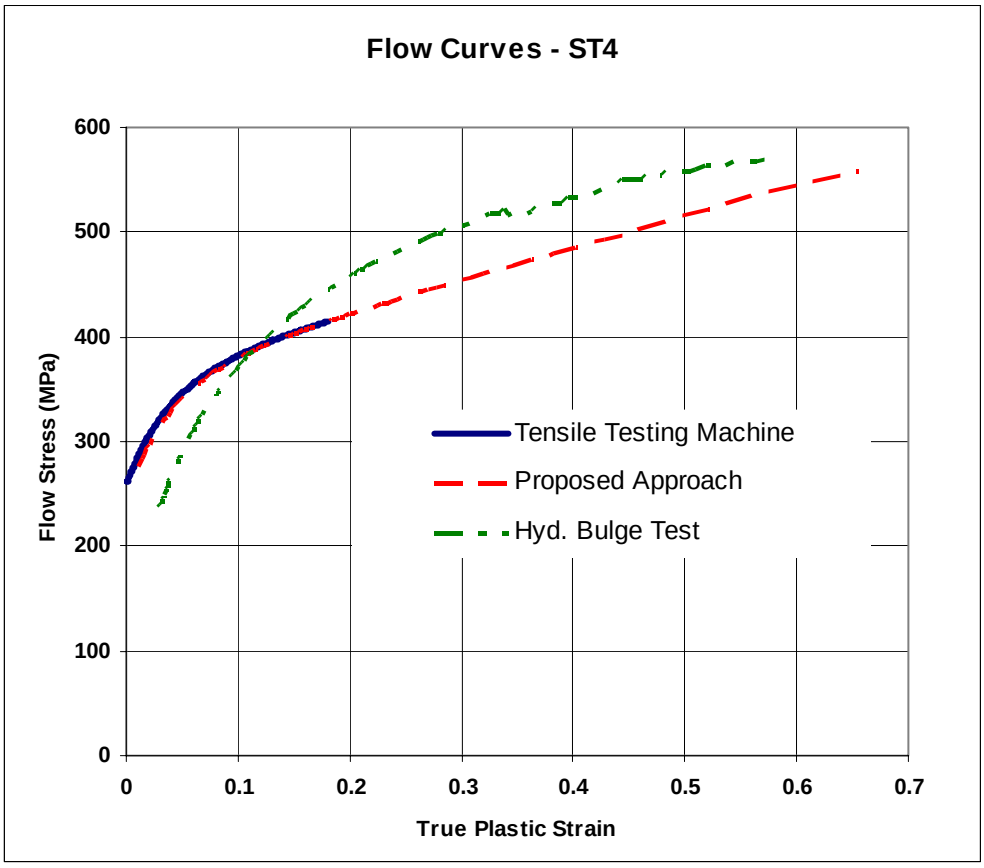

Figure 4.9 Flow curves of ST4 evaluated by various methods

CHAPTER 5

CONCLUSIONS

Plastic properties of materials are needed for the theoretical and numerical modeling of metal forming processes. Using the plasticity theory in the development of theoretical models, relationship between the equivalent-stress and equivalent-strain must be known. In order to calculate the forces required for metal forming processes it is necessary to know the stress-strain curve of the metals to be formed. The final dimensions and stress-strain distribution of the specimens have to be obtained from the modeling of experiments very close to reality. Therefore it is very important to obtain flow curves correctly.

Tension test is the most common test, but supplies a flow curve up to strain values reached at the beginning of necking . This study is mainly focused on determination of flow curves up to strains where rupture initiates.

Experimental works of the study consist of large strain flow curve of sheet metals, determination of the using genereted computer code and HBT. Besides, genereted flow curves are simulated to obtain experiemental parameters. Tensile tests are conducted according to ASTM E-8 standarts.

A direct approach of obtaining flow curves from tension tests using optic strain measurements is introduced. The simplicity, elegance and the speed of the introduced direct approach has the cost of assuming that the strains measured by Gom-Aramis System are totally plastic. Despite this rough assumption, simulation of the tension test provides a very close extension-force diagram to the experimental curve when the flow curve produced by the introduced approach is used.

It is observed that the tension test provides higher equivalent strains when compared to hydraulic bulge test of the same material. It is interesting to see that there exists a ramp up towards the end of the flow curve. It is not common that well-known flow curve approximations provide such behaviour.

The approach may be improved by an optical strain measurement system which is capable of measuring the width of the specimen completely. Although the approach has conceptually a solid ground, these early results should be extended by more experiments and verifications. Furthermore, the elastic-plastic decomposition of strains measured by the optic measurement system is still remains as a further study.

Another further study would be this: the applicability of the proposed technique is restricted to isotropic material responses, its extension to anisotropic materials may also be possible by among different possibilities, including anisotropic effect in the yield criterion and plastic flow rule.

As a conclusion, this study covers both numerical and experimental works about material characterization (based on the tension test) and determination of large stain flow curve of sheet metals.

REFERENCES

[1] Taylan Altan et al., 2005, Cold and Hot Forging Fundamentals and Applications.

[2] William F. Hosford, 2005, Mechanical Behavior of Materials.

[3] David Roylance, 2001, Department of Materials Science and Engineering Massachusetts Institute of Technology Cambridge Stress-Strain Curves.

[4] Serope Kalpakjian, 2002, Manufacturing Processes for Engineering Materials.

[5] J,R Davis, 2004, Tensile Testing Second Edition.

[6] J. M. Alexander and R. C. Brewer, 1968, Manufacturing Properties of Materials.

[7] Özgür Koçak, 2003, Analysis Formability of the Metals.

[8] Gerhard Gutscher et al., 2003, Determination of flow stress for sheet metal forming using the viscous pressure bulge (VPB) test.

[9] Chakrabarty and Alexander, 1970, Hydrostatic bulging of circular diaphragms.

[10] M. Atkinson, 1996, Accurate determination of biaxial stress–strain relationships from hydraulic bulging tests of sheet metals, Int. J. Mech. Sci. 39 (7) (1996), pp. 761–769.

[11] G. Gutscher, 2004, Determination of flow stress for sheet metal forming using the viscous pressure bulge (VPB) test, pp. 1–7.

[12] P. Broomhead and R.J. Grieve, 1982, Effect of strain rate on the strain to fracture of a sheet steel under biaxial tensile stress conditions, pp. 102–106.

[13] A.K. Pickett, 2004, Failure prediction for advanced crashworthiness of transportation vehicles, pp. 853–872.

[14] V. Grolleau, 2008, Biaxial testing of sheet materials at high strain rates using viscoelastic bars, pp. 293–306.

[15] E.Verhulp, 2003, A three-dimensional digital image correlation technique for strain measurements in microstructures.

[16] M. Jerabek, 2010, Strain determination of polymeric materials using digital image correlation.

[17] H.W. Schreier and M.A. Sutton, 2002, Systematic errors in digital image correlation due to undermatched subset shape functions.

[18] Y.F. Sun and H.J. Pang, 2007, Study of optimal subset size in digital image correlation of speckle pattern images.

[19] D. Tscharnuter et al., Poisson's ratio of polypropylene and polypropylene compounds in various strain histories, submitted for publication.

[20] F. Grytten et al., 2009, Use of digital image correlation to measure large-strain tensile propertiesof ductile thermoplastics.

[21] Jinlong Chen et al., 2009, Deformation measurement across crack using two-step extended digital image correlation method.

[22] S. Dumoulin et al., 2002, Determination of the equivalent stress–equivalent strain relationship of a copper sample under tensile loading.

[23] Qin-Zhi Fang et al., 2008, Effect of cyclic loading on tensile properties of PC and PC/ABS.

[24] Fabienne Lagattu et al., 2004, High strain gradient measurements by using digital image correlation technique.

[25] Y. H. Zhao et al., 2009, Influence of specimen dimensions and strain measurement methods on tensile stress–strain curves.

[26] Julien Réthoré et al., 2007, From pictures to extended finite elements: extended digital image correlation (X-DIC).

[27] V. Tarigopula et al., 2007, A study of localization in dual-phase high-strength steels under dynamic loading using digital image correlation and FE analysis.

[28] F.M. Sánchez-Arévalo and G. Pulos, 2008, Use of digital image correlation to determine the mechanical behavior of materials.

[29] Sören Ehlers and Petri Varsta, 2009, Strain and stress relation for non-linear finite element simulations.

[30] ASTM E8 / E8M -09 Standard Test Methods for Tension Testing of Metallic Materials

[31] Zwick//Roell Z300E User Documentations.

[32] GOM - Aramis Optical Measurement System User Documentations.

[33] M. Sutton et al., 2000, Advances in two-dimensional and three-dimensional computer vision, Photomechanics 323–372.

[34] V. Tiwari et al., 2009, Application of 3D image correlation for full-field transient plate deformation measurements during blast loading, International Journal of Impact Engineering 36 (6) 862–874.

[35] Koç M., Aueulan Y., Altan T., 2001, On the Characteristics of Tubular Materials for Hydroforming – Experimentation and Analysis. International Journal of Machine Tools and Manufacturing; 41(5):761–72.

[36] Pavlina E. J., Van Tyne C.J., Hertel K., 2008, Hydraulic Bulge Testing of Dual Phase Steel Tubes Produced using a Novel Processing Route. Journal of Material Processing Technology; 201:242–6.

[37] Çelik Gökhan, 2010, Experimental Investigation of Influence Parameters on Forming Limit Diagrams of Aluminum alloys.

[38] Velasco R, Boudeau N., 2008, Tube Bulging Test: Theoretical Analysis and Numerical Validation. Journal of Material Processing Technology; 205:51–9.

[39] Ceretti E., Braga D., Giardini C., 2008, Steel and Copper Flow Stress Determination for THF Applications. Int J Mater Form; 1:309–12.

[40] Hwang Y-M., Lin Y-K., Chuang H-C., 2009, Forming Limit Diagrams of Tubular Materials by Bulge Tests. Journal of Materials Processing Technology; 209:5024–34.

APPENDIX A

Table A.1 Properties of Z300E tensile testing machine

BUP600 Hydraulic Press	Specifications
Max. Force (kN)	300
Max. Speed (mm/min)	250
Max. Sheet Metal Thickness (mm)	16
Max. Sheet Metal Width (mm)	20
Extensometer	Tangible
Gage Length	L0+L0*80%

Table A.2 Properties of BUP600 hydraulic press

BUP600 Hydraulic Press	Specifications
Max. Ram Force (kN)	600
Max. Clamping Force (kN)	600
Max. Ram Speed (mm/min)	750
Punch Diameter (mm)	120
Max. Sheet Metal Thickness (mm)	10
Max. Sheet Metal Width (mm)	260

Table A.3 Test parameters for HBT

Test Parameters	
Max. Ram Force (kN)	400
Clamping Force (kN)	100
Ram Speed (mm/min)	2,50
Ram Diameter (mm)	120
Sheet Metal Thickness (mm)	1,5-1,8
Sheet Metal Diameter (mm)	130
Shutter Time of Optical Device	16
Frame Rate of Optical Device (Hz)	20

Table A.4 Tension test terminology [37]

TENSILE TEST TERMINOLOGY	
Engineering Stress & Strain	Maximum tensile strength can be defined as maximum stress that material can withstand without breaking or failing. It can simply be found by dividing the maximum load with instantaneous cross sectional area. Ultimate tensile strength (UTS) is another commonly used term for tensile strength.
True Stress & Strain	True stress is more useful for engineering applications. It gives more direct measure for plastic response of material since it uses final length of the specimen. Engineering stress-strain data must be converted to true stress-strain data before it is used.Strain measurement is often used in conjunction with true stress data that takes the incremental increase in displacement not the original one.
Yield Point	Yield point is the point which shows the end of elastic deformation. Plastic deformation starts with yield point so that if permanent shape change is desired, yield point must be exceeded. The way from yield point to ultimate strength is significant because it determines amount of attainable plastic strain. Yield point is also a factor that is used to determine springback behavior.
Elongation	Elongation shows the total increase in specimen's length from yield point to fracture (rupture). Total elongation is determined by broken and original specimen measurements. In general, metals elongate 30-50%. Elongation does not show formability because for the same material with different specimens, elongation may change.
Yield Point Elongation	In a uniaxial test, the strain (expressed in percent) separating the stress-strain curve's first point of zero slope from the point of transition from discontinuous yielding to uniform strain hardening.
Tensile Strength	Maximum tensile strength can be defined as maximum stress that material can withstand without breaking or failing. It can simply be found by dividing the maximum load with instantaneous cross sectional area. Ultimate tensile strength (UTS) is another commonly used term for tensile strength.

Table A.5 Some assumptions on different element types in FE [37]

ELEMENT TYPE	ASSUMPTION
Thin Shell Elements	• 6 DOF's (including translations and rotations) • Thickness is required as an input • Ignores out-of-plane normal stress • Ignores out-of-plane transverse shear stress • Very small thickness (smaller than 0.05 mm)
Thick Shell Elements	• 6 DOF's (including translations and rotations) • Thickness is required as an input • Ignores out-of-plane normal stress • Considers out-of-plane transverse shear stress • Small thickness (smaller than 0.1 mm and greater than 0.05 mm)
Membranes	• 3 DOF's (only translational motions) • Applicable to in-plane loadings only in planar and curved surfaces • Tension space structure covering
Shear Panel Elements	• 3 DOF's (only translational motions) • It is an idealized model of elastic sheets • Restricted to linear materials • Large displacement effects are neglected • Evaluates only shear stresses at all four nodal points
Axisymmetric Shell Elements	• 3 DOF's (2 translational motions and 1 rotation) • Only in-plane loading are applied • Suitable for large displacements and large membrane strains

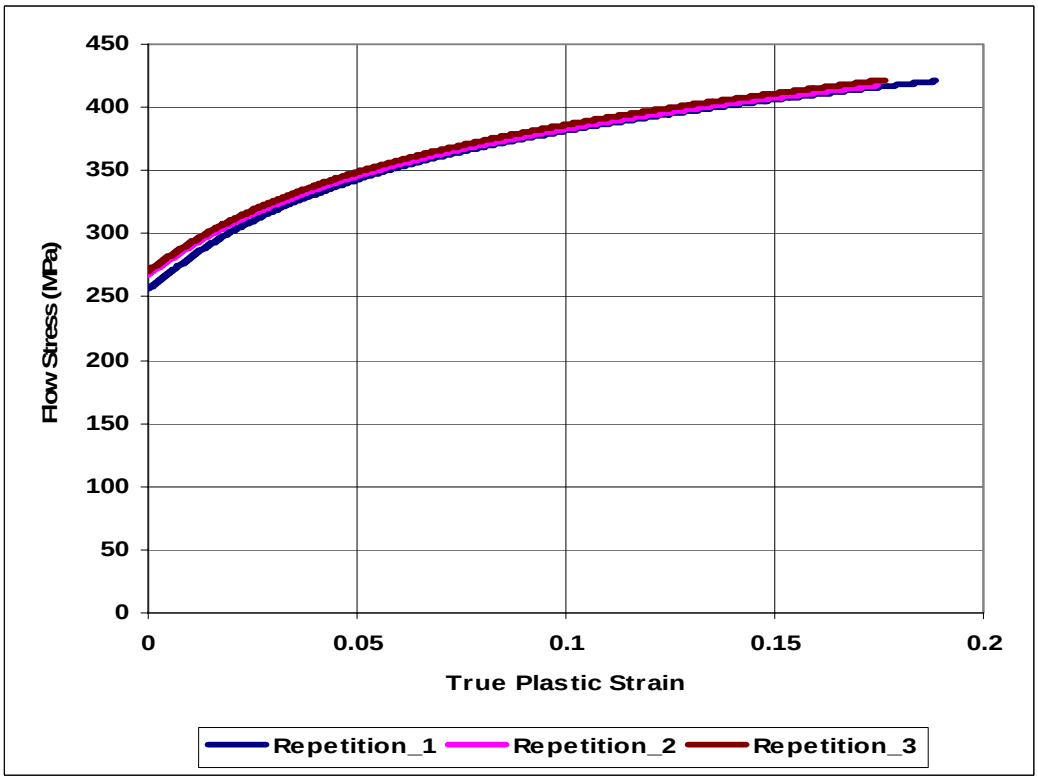

Figure A.1 Flow curve repetitions of ST12

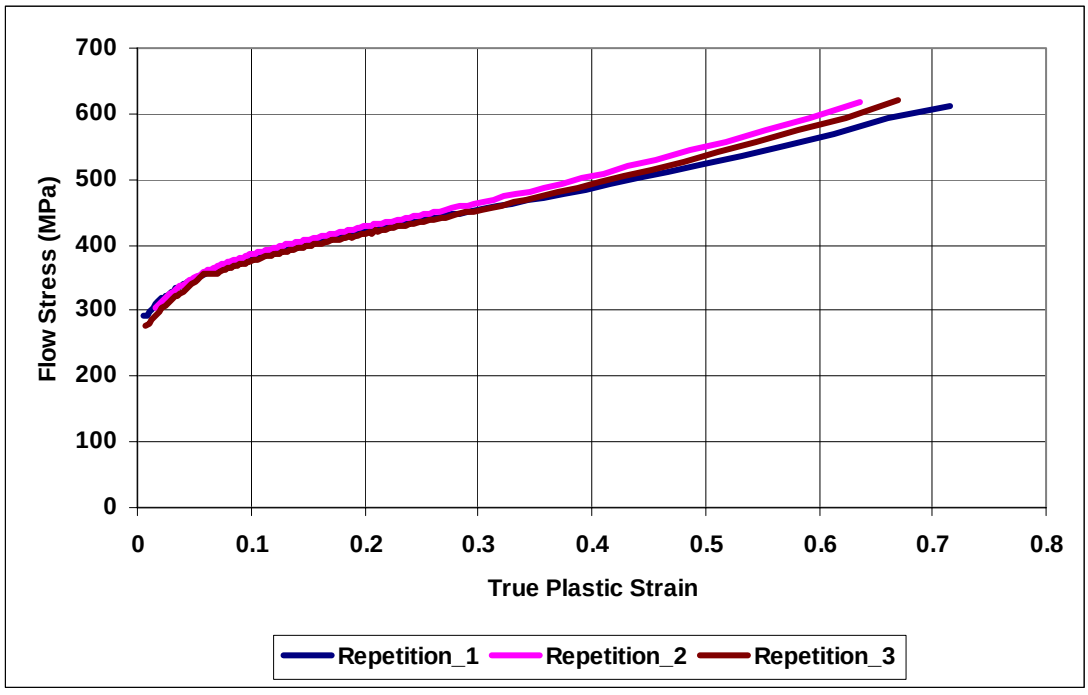

Figure A.2 Proposed approach flow curve repetitions of ST12

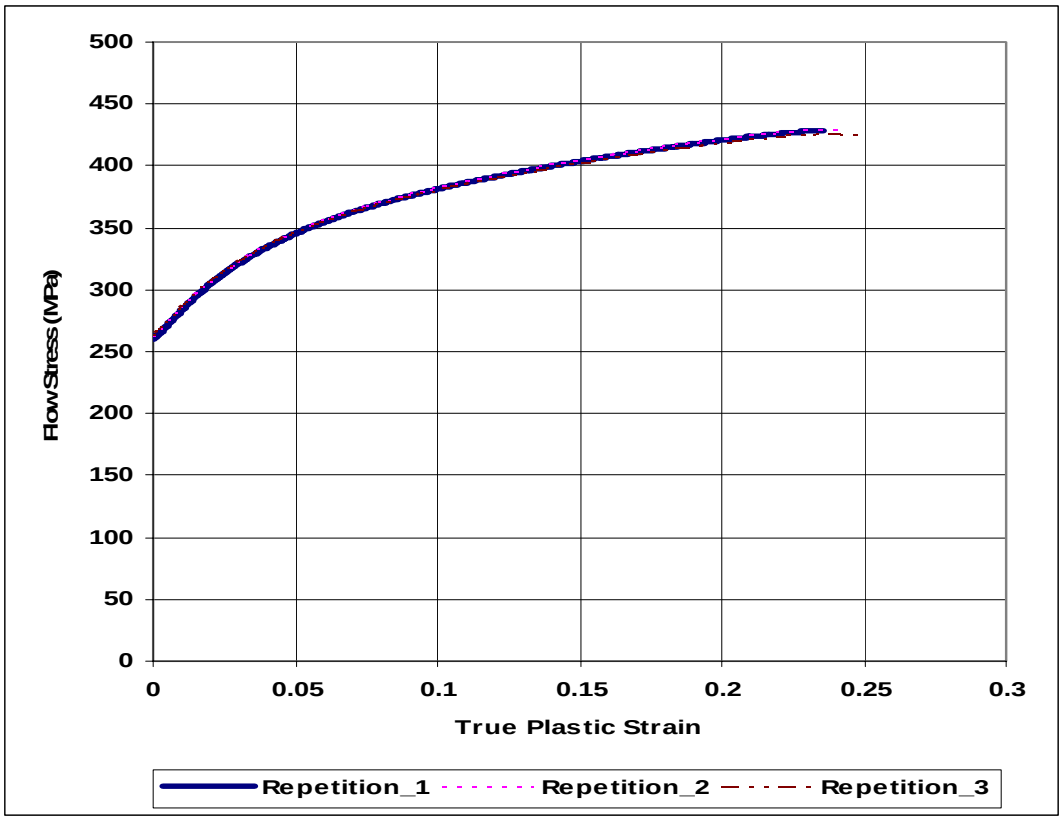

Figure A.3 Flow curve repetitions of ST4

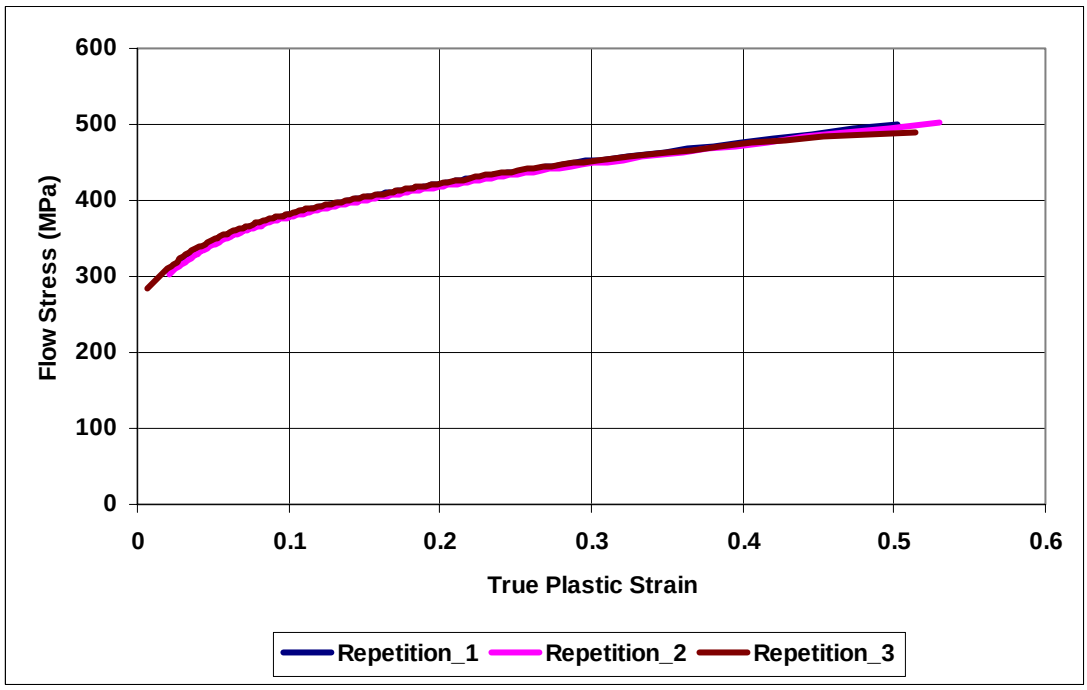

Figure A.4 Proposed approach flow curve repetitions of ST4

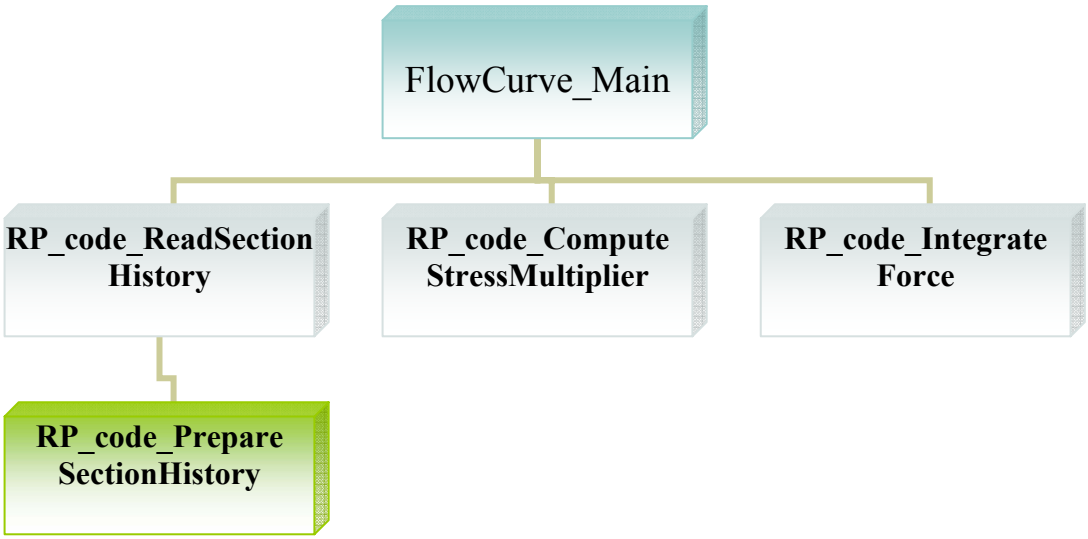

Figure A.5 The order of functions is called up by generated computer code